Astron. Astrophys. 169, 14–42 (1986)

ASTRONOMY AND ASTROPHYSICS

A high resolution hydrogen-line survey of Messier 31

III. H I holes in the interstellar medium

E. Brinks[1,3] **and E. Bajaja**[2,1,★]

[1] Sterrewacht Leiden, Postbus 9513, NL-2300 RA Leiden, The Netherlands
[2] Instituto Argentina de Radioastronomía, Casilla de Correo No. 5 (1894), Villa Elisa (Pcia. de Bs. As.), Argentina
[3] European Southern Observatory, Karl-Schwarzschild-Straße 2, D-8046 Garching bei München, Federal Republic of Germany

Received February 7, accepted June 4, 1986

Summary. Inspection of the high resolution H I survey of M 31 made recently with the Westerbork SRT has revealed regions which are depleted of H I, H I holes. The sizes of these holes range from about 100 pc, a limit set by the size of the beam, to 1000 pc. Some show a shell structure. Most holes lie in a broad annulus with a radius of 10 kpc, i.e. in the area with the highest H I column density and highest number density of H II regions and OB-associations. The H I masses which are estimated to be absent at the position of H I holes range from about $10^3\ M_\odot$ to $10^7\ M_\odot$. The energy needed to produce the holes lies in the range from 10^{49} to 10^{53} erg. Kinematic ages are derived which lie between 2.5 and 30 10^6 years. The H I holes smaller than 300 pc are correlated with OB-associations and H II regions. For the larger holes a similar correlation is suggested by the data but no firm statement can be made due to the high probability for overlapping in the broad annulus around 10 kpc. The production rate for holes is 1 per 10^5 years. Assuming an average of 10^2 supernovae per year, we derive a lower limit for the supernova rate of $10^{-3}\ \mathrm{yr}^{-1}$ or $10^{-14}\ \mathrm{pc}^{-3}\ \mathrm{yr}^{-1}$, an order of magnitude lower than the corresponding local value for the Galaxy. The filling factor for the holes is only 1 %. This is much less than the filling factor for the hot low density medium in the Galaxy according to the McKee and Ostriker model and suggests that the hot gas in M 31 does not form a tunneling network.

Key words: galaxies: M 31 – galaxies: structure of – interstellar medium: bubbles – radio lines: 21-cm

1. Introduction and observations

The recent high resolution survey of M 31 in the line of neutral hydrogen made with the Westerbork Synthesis Radio Telescope (WSRT) has revealed structures in the H I which, by their appearance in the maps are best referred to as H I holes (Brinks and Shane, 1984; henceforth Paper I). These holes are characterized by a relative absence of neutral hydrogen, they have typical dimensions of 100 pc to 1 kpc, and they appear roughly circular on the maps, indicating that their three dimensional shape is more or less spherical. Because the resolution of the survey $\Delta\alpha \times \Delta\delta \times \Delta V = 24'' \times 36'' \times 8.2\ \mathrm{km\ s^{-1}}$, corresponding, at the assumed distance of M 31 of 690 kpc, to a linear resolution of 80 pc × 120 pc, does not allow us in general to resolve the boundary layers of these features, we prefer to refer to the structures as holes instead of H I shells or bubbles. Only a few holes show a clear shell structure and deserve the name H I shell. An example of an H I hole, which coincides with the bright OB-association NGC 206 (OB78 in the list of OB-associations published by van den Bergh, 1964) has been discussed by Brinks (1981) and a preliminary analysis of some other holes has been given by Brinks and Bajaja (1983a, b).

The H I holes in M 31 show similarities with the H I shells and supershells which have been found in the Galaxy by Heiles (1979, 1984), and with the giant and supergiant shells in the LMC described by Meaburn (1980, and references cited therein). Also, recent H I observations of yet another member of the Local Group, M33, show a multitude of H I holes similar to the findings in M 31 (Deul, private communication). Finally observations of the irregular galaxy IC10 by Shostak and van Woerden (1983) clearly demonstrate the presence of H I holes with typical dimensions of a few hundred parsecs and presumably expansion velocities of about 10–20 km s^{-1}.

The observations mentioned above suggest that H I holes in galaxies are a general phenomenon and that they fill an appreciable fraction of the interstellar space. There is evidence that H I holes are related to OB-associations as discussed for example by Heiles (1979). He found, in the Galaxy, a weak general correlation of H I shells and supershells with OB-associations, despite the fact that interstellar extinction severely hampered his analysis. Some H I shells are clearly correlated with an OB-association like Orion's cloak and Carina (Cowie et al., 1979, 1981) and some are sources of X-ray emission like the super bubble in Cygnus (Cash et al., 1980). In the case of the LMC, Meaburn (1980) has shown that the well-defined supergiant shells LMC 1, 4, and 5, which are traced by their Hα + [N II] emission, coincide with regions which are devoid of neutral hydrogen, H I holes, and that they contain several tens of OB stars which are a source of UV radiation. Braunsfurth and Feitzinger (1983) discuss the correlation between OB-associations and ring-shaped emission regions in the LMC. From the [S II]/Hα line ratios Georgelin et al. (1983) reach the conclusion that ionized bubbles are most probably old H II regions inside which supernova explosions have occurred.

Send offprint requests to: E. Brinks (ESO)

★ Member of the Carrera del Investigador Científico of the Consejo Nacional de Investigaciones Científicas

Table 1a. General information on M 31

Position of the optical nucleus and line of nodes	$\alpha_{1950} = 0^h40^m00^s.28$ $\delta_{1950} = 40°59'42''.9$ $\theta_{1950} = 37°46'.6$	Baade and Arp (1964), precessed to 1950.0
Galactic coordinates	$l = 121°.18$ $b = -21°.57$	de Vaucouleurs et al. (1976)
Systemic velocity	$-315\ \mathrm{km\,s^{-1}}$	Brinks and Burton (1984)
Inclination	77°	Brinks and Burton (1984)
Distance	690 kpc[a]	Baade and Swope (1963)

[a] At this distance 1′ corresponds to 200 pc

Table 1b. Instrumental and map data

Right ascension of map centre	(1950.0)	$0^h40^m00^s$
Declination of map centre	(1950.0)	41°00′
Average HPBW ($\Delta\alpha \times \Delta\delta$)	(arcsec)	24 × 36
Channel velocities	($\mathrm{km\,s^{-1}}$)	−618.1 (4.1) −16.2
Velocity resolution	($\mathrm{km\,s^{-1}}$)	8.2
Average system noise	(K)	90
R.m.s. noise in a channel	(mJy)	2.8
Flux equivalent of 1 K	(mJy)	1.39
Frequency taper		Hanning
Polarization direction		East-West
HPBW of primary beam	(arcmin)	37.6

Several models exist, describing the evolution of an OB-association and its effects on the surrounding interstellar medium, which attempt to explain the H I holes (or shells or bubbles). Tenorio-Tagle et al. (1982) and Tenorio-Tagle (1984) show how during a certain phase in the evolution of an H II region surrounding an OB-association an expanding thick neutral shell can be formed. Their model predicts shells of a few hundred parsecs in radius. It neglects the influence of stellar winds.

Bruhweiler et al. (1980) and Tomisaka et al. (1981) combine in slightly different approaches earlier work on the energetics of wind-driven interstellar bubbles (Castor et al. 1975; Weaver et al., 1977) and single supernova explosions (Chevalier, 1977). In their models first a cavity is created due to the strong stellar winds of the massive stars in the associations. After a certain time the most massive stars become supernovae and shells as observed by Heiles (1979) are produced. Once shells have been formed according to one of the models listed above, radiation pressure from field stars can cause runaway expansion of the shells which leads to the formation of supershells (Elmegreen and Chiang, 1982). Another method to create the supershells has been put forward by Tenorio-Tagle (1981), who suggests that they might result from the collision of high velocity clouds with a galactic disk.

In all models the interstellar medium is supernova dominated and regions filled with hot low density gas are in pressure equilibrium with cooler gas. Cox and Smith (1974) realised that a supernova rate of the order of 1 per 50 years in the gaseous disk of our Galaxy is sufficient to generate and maintain throughout the interstellar medium a network of interconnected tunnels filled with low density ($n \lesssim 10^{-2}\ \mathrm{cm^{-3}}$), high temperature ($T \sim 10^6$ K) gas. This was worked out in detail by McKee and Ostriker (1977) who describe the interstellar medium as a three component medium. The largest fraction is filled with hot gas in which cool clouds with warm envelopes are embedded.

The work presented here is based on the new high resolution H I survey of M 31, performed with the Westerbork Synthesis Radio Telescope (WSRT). Table 1a supplies some general data on M 31 and Table 1b summarizes the instrumental and map data. A full account of the observations, the calibration, and the data reduction is given in Paper I. The observations were made using the WSRT in its 1.5 km configuration. Five fields were needed, which were subsequently combined into a single map, to cover most of the optical image of M 31. On the major axis the measurements extend to 15 kpc from the nucleus. As is described in Paper I, various sets of maps were produced. The data sets which will be frequently referred to during the rest of this paper are:

Set I: A series of 147 channel maps at a resolution of $\Delta\alpha \times \Delta\delta \times \Delta V = 24'' \times 36'' \times 8.2\ \mathrm{km\,s^{-1}}$ and separated in velocity by $4.1\ \mathrm{km\,s^{-1}}$. This set corresponds to data set (a) from Paper I. Because the maps are corrected for the primary beam attenuation, the noise varies across the maps. The maximum noise is found at the extreme northern and southern ends of the major axis. Masks are applied, as described in Paper I, which set to zero all intensities outside the regions containing H I.

Set II: As Set I, but multiplied by the combined primary beam attenuation to create equal-noise maps in which the noise level is constant across the map. The sensitivity varies according to the combined primary beam attenuation pattern. (See Paper I for a detailed description.) No masks are applied to this set of channel maps.

These two sets were used to compile a catalogue of H I holes in M 31. This catalogue is described in Sect. 2. Section 3 is devoted to the analysis of the properties of the holes and Sect. 4 to the correlation of H I holes with H II regions and OB-associations. In Sect. 5 we discuss our results and we summarize our conclusions in Sect. 6.

2. Catalogue of H I holes

The H I holes can be clearly recognized on the channel maps of the H I survey. One can identify numerous such features in the maps presented as Fig. 6 in Paper I. However, this method of recognizing H I holes is subjective and depends strongly on the way the H I emission is perceived by the human eye and the readiness of the brain to accept structures such as holes and shells. To perform an unbiased search for holes one would need a complex pattern recognition algorithm. Hu (1981) has shown that for the high latitude H I survey of the Galaxy by Heiles and Habing (1974) an unbiased search is possible. She was able to enhance features such as H I holes and shells by applying a special purpose filter in velocity space, making use of the fact that the H I shells are well peaked in velocity compared to the background which varies only slowly with velocity. Her method proved unsuccessful for M 31 because, as we will see later in this paper, the boundary between the hole and surrounding H I is smeared out by our beam of about 100 pc, reducing the sharpness of the edge of the hole. Secondly, the velocity resolution is too coarse or, in other words, the overall H I distribution changes so much from channel to channel that one cannot treat the background as slowly varying.

Further, the maps presented in Figs. 7 and 8 in Paper I show the presence of two or sometimes more H I structures along the line-of-sight. In the second paper in this series, Brinks and Burton (1984, Paper II) show that a splitting into two velocity systems can be understood by assuming that the H I in M 31, at large galactocentric distances, bends away from the plane of the disk, i.e. that M 31 has a warp. Thus the contrast of an H I hole which is located in the disk of the galaxy is reduced when one adds the maps over the full velocity range to produce a total surface brightness map. This is analogous to the situation in the Galaxy where, along a line-of-sight, many H I structures are added to form a complex spectrum. This led Heiles (1979) to use "velocity slices" or channel maps to search for the H I shells. Because of this blending of velocity structures and because our data set has not enough resolution to apply an unbiased search algorithm as proposed by Hu we decided to use the channel maps, where the integration is over a small range in velocity only.

The maps which were used to search for H I-holes were those of Set II because these maps, which are not corrected for the primary beam attenuation, render the search uniform in terms of the general noise level. The search for H I-holes was conducted on the Leiden image processing system. Five consecutive channel maps were loaded each time into the memory of the system and displayed in sequence as a short film-loop on the display monitor. Because this method is necessarily subjective we took great care to minimize any personal bias, and we applied selection criteria which a candidate object should meet before it was accepted as an entry in the catalogue. The selection criteria applied were:

i) An H I hole must be clearly visible in at least three successive channel maps. This condition insures that we not be misled by features which are the result of chance arrangements of pixels. The minimum of three consecutive channel maps is chosen because the frequency data were Hanning tapered during the observations which means that neighbouring channels are correlated.

ii) The centre of an H I hole must be stationary in the channel maps in which it is seen. This requirement should separate genuine holes, which correspond to density variations, from pseudo-holes which find their origin in kinematical effects.

iii) The hole must have a good contrast with respect to its surroundings in all relevant channel maps. This was checked by plotting intensity profiles along two perpendicular cuts through the centre of each hole. An a posteriori quantification is presented in the next section.

iv) The shape of the hole must be clearly definded and adequately described by an ellipse.

To reduce personal bias, an independent list of candidate objects was compiled by both authors separately. The candidate objects were given quality ratings, Q, indicating to what degree the above criteria were met. After completion the two lists were compared and combined. The same procedure was followed for candidate objects in the total H I map (see Fig. 9, Paper I). Although one might expect to find objects in this map which are not seen in the channel maps, for instance holes which are larger than the typical H I extent on a single channel map, or very diffuse ones, or holes which have a low contrast in the channel maps but which contain reduced H I over the full velocity range, no features were found which were not already on the list.

I making our list it proved that criteria iii) and iv), both subjective, had a rather large influence on the quality rating Q. More serious is that the quality assigned to an object also depends on the brightness and contrast setting of the monitor. Furthermore it appeared that in the course of examining the objects, our rating slowly changed. Therefore all objects in the provisional list were examined once again. During this final inspection we were assisted by Mrs. H. Versteege-Hensel, who served as an unbiased referee. From the inspection of the objects on the image processing system we obtained the position of the object, accurate to about $0\rlap{.}'1$ (one picture element), the velocity of the channel map in which it was defined best and a final quality rating, Q, ranging from 1 to 3 (highest quality). It should be emphasized that this final list of H I holes is based solely upon the H I survey and is not biased in any respect by other information like the location of H II regions, SNRs, OB-associations etc. The search for H I holes covered the full extent of the WSRT survey of M 31, i.e. most of the optically prominent part of this galaxy.

For each H I hole in this final list we produced the following set of pictures:

– an H I spectrum at the centre of the hole,
– two cuts through the centre of the hole, one parallel to the major axis and the other parallel to the minor axis of M 31, through the channel map on which the hole is best defined. Each cut has a length of 9′,
– a set of position-velocity maps along the same lines and plotted on the same scales as the cuts and the spectrum,
– two cuts, along the same lines, made through the total H I surface density map, again on the same scale,
– a gray-scale picture of the channel map on which the hole is best seen showing the region containing the hole with a contour drawn at the 50% contrast level (see below).

The pictures described above were, except for the cuts through the integrated H I map, based on the maps of Set I. Figures 1–4 show these sets of pictures for some typical examples of H I holes listed in our catalogue. The spectrum gives an indication of the velocity range over which the H I and the hole are seen. The cuts through the channel maps (panels d and e) show the contrast of the hole with respect to its surroundings. For each hole the depth was measured as illustrated in Fig. 4e and the intensity which corresponds to 50% of the total decrease in brightness was determined. A map of a small region centered on the hole was produced from the channel which corresponds to the velocity at

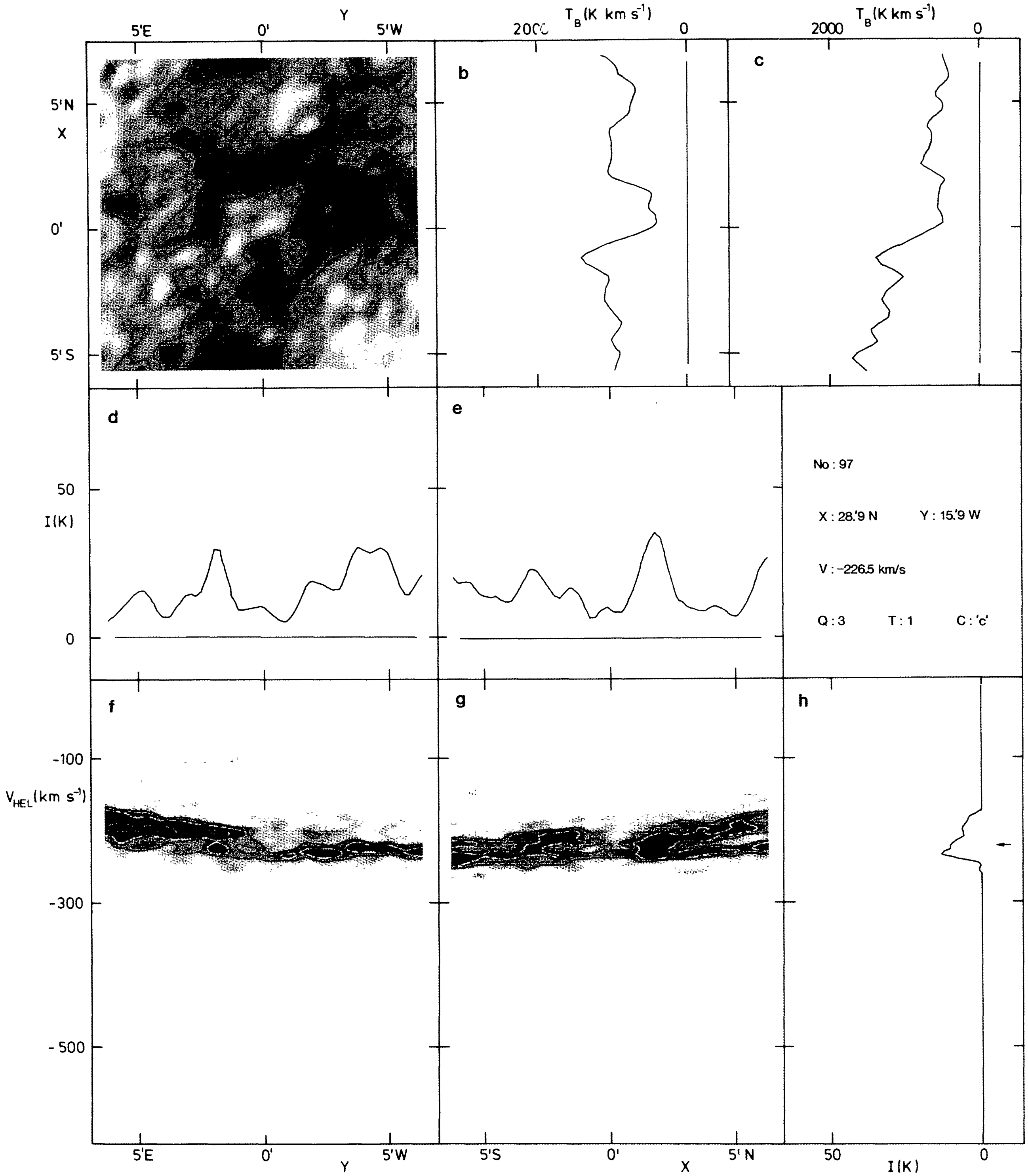

Fig. 1. Collection of pictures for hole 97 which were used to derive some of the properties of the hole as described in the text. The panels show the following: a) expanded view of the channel map on which the hole is seen best. The contour level is drawn at 12.0 K which corresponds to the 50% depth level of the hole. b) and c) are the cross-cuts, plotted on the same linear scale as the channel map, made parallel to the X- and Y-axes respectively, through the total surface brightness map; d) and e) are the cuts made along the same lines and on the same scale through the channel map shown in panel a); f) and g) are position-velocity maps made along the same cuts and on the same linear scale. The contour levels are 10.0, 20.0, 40.0, and 60.0 K; h) shows the spectrum made at the centre of the hole. The arrow indicates the velocity at which the hole is best seen

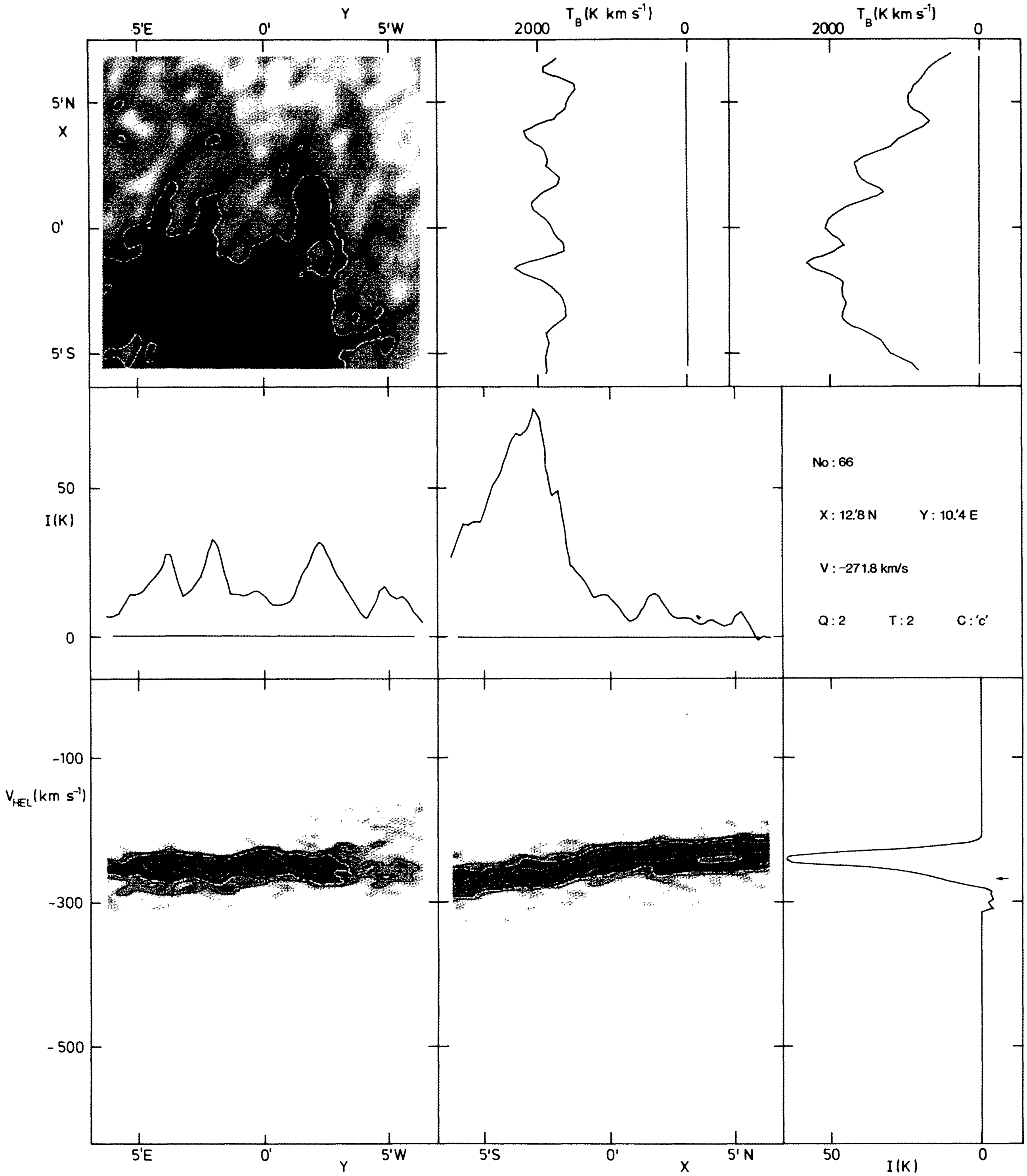

Fig. 2. As Fig. 1 but for hole 66. The contour level in the channel map is 20.0 K

which the hole is best seen (panel a). Gray scales are used to indicate the brightness levels in the map and a contour is drawn at the 50% contrast level. In this map an ellipse is fitted by eye to the 50% contour as a measure of the full width of the hole at half depth. The catalogue lists the minor diameter, the major diameter and position angle of this ellipse, uncorrected as yet for smoothing by the WSRT beam. In a later stage we corrected these values for the beam. Depending on the smoothness of the 50% contour, the given dimensions of the hole usually have an accuracy of 0.′1. Because the synthesized beam is elongated in the declination direction, most holes have an apparent position angle close to 0°. A reliable value for the position angle can therefore only be given for

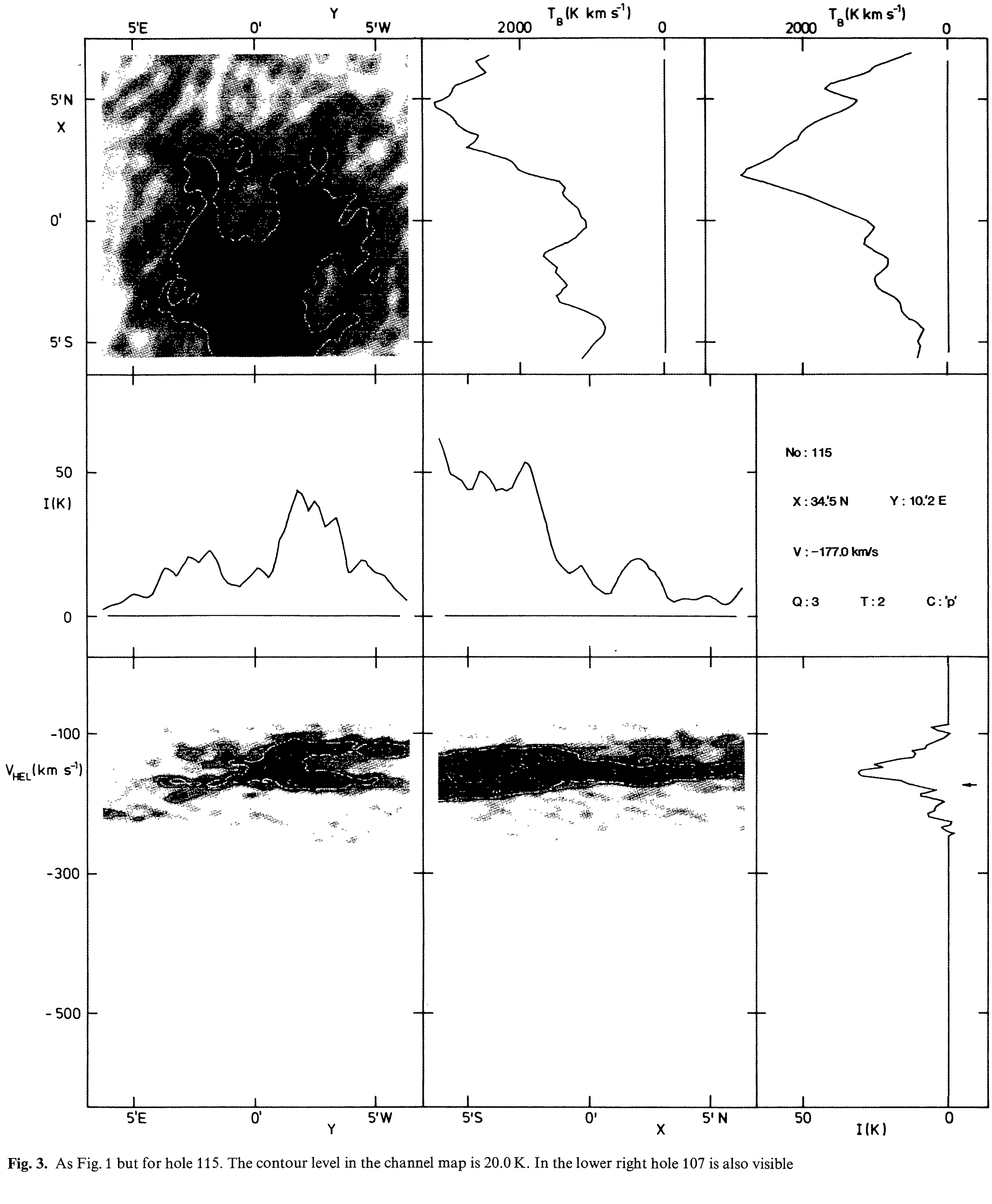

Fig. 3. As Fig. 1 but for hole 115. The contour level in the channel map is 20.0 K. In the lower right hole 107 is also visible

those holes where its value is clearly different from 0°. Further the channel maps are used to differentiate between holes which are on all sides surrounded by H I or class "*c*" holes, and holes which are only partially surrounded or class "*p*".

The two position-velocity maps, panels f and g, add another important piece of information to the properties of the H I holes, i.e. their signature in velocity space. According to their appearance on these maps we are able to divide the holes into three types, Type 1, 2, and 3. A hole is classified as Type 1 if it is clear from the position-velocity maps that, at the position of the hole, H I is absent over the full velocity range. If the position-velocity maps show two distinct velocity systems, e.g. the disk and the warp, this H I

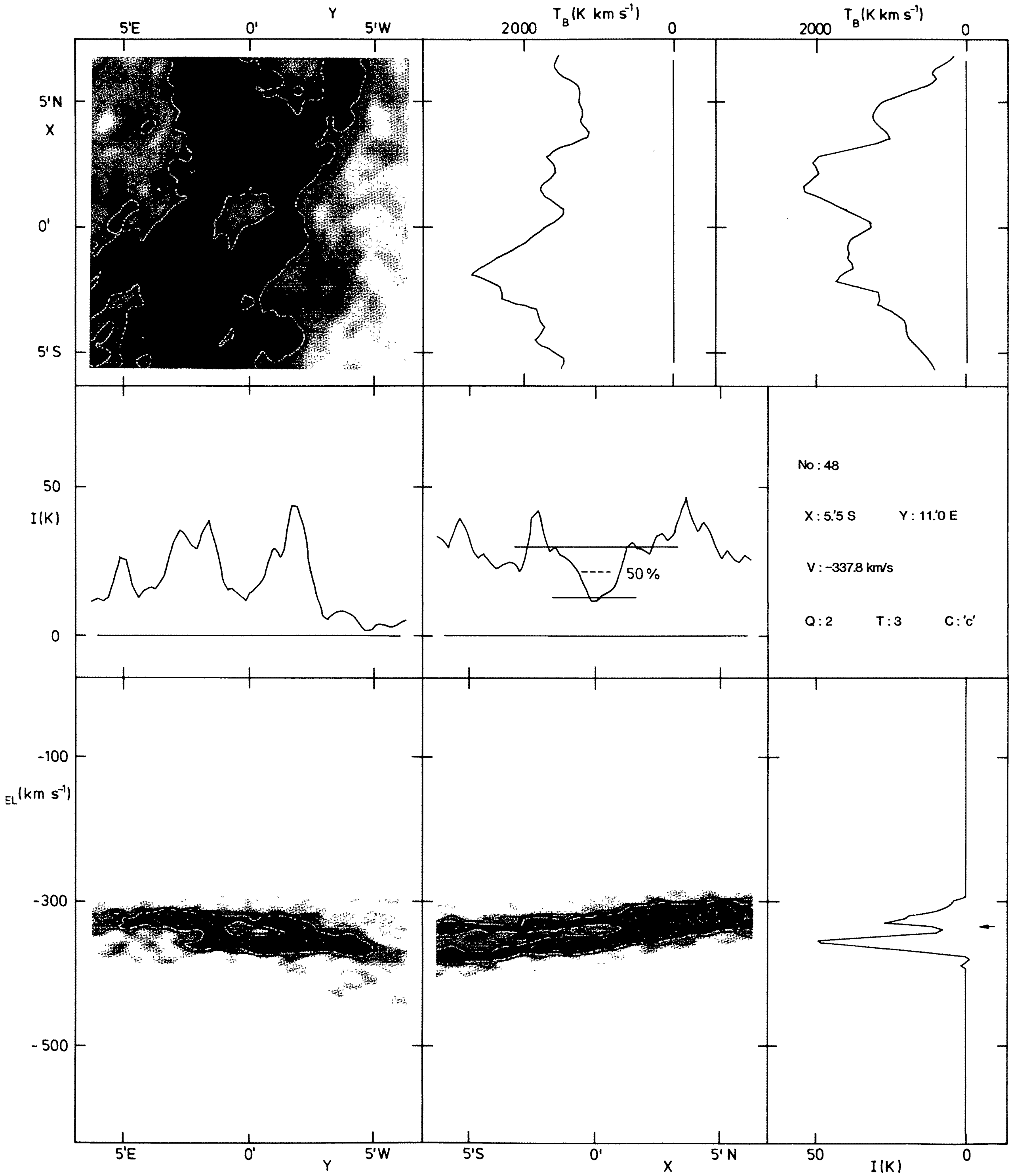

Fig. 4. As Fig. 1 but for hole 48. The contour level in the channel map is 20.5 K

deficiency refers only to that velocity structure, normally the disk, to which the hole belongs. Figure 1 is an example of a Type 1 hole. The Type 2 hole is characterized by a shift of the H I at the position of the hole to a higher or lower velocity. This is illustrated by the position velocity maps shown in Figs. 2 and 3. In Fig. 2 the H I is shifted by 21 km s^{-1} to a higher radial velocity. In case of a Type 2 hole this velocity shift, DV, is listed as a negative number if the H I is blue-shifted with respect to the velocity expected at the position of the hole and as a positive number if it is red-shifted. In a Type 3 hole the H I structure shows a clear splitting into two components, one blue-shifted and one red-shifted. An example is shown in Fig. 4. The velocity difference between red-shifted and blue-shifted

H I divided by two is listed as DV and is interpreted as the expansion velocity of the shell or of the ambient H I surrounding the hole.

The final property which is determined for each hole is the ambient volume density of H I. This value is obtained by estimating, from the profiles through the integrated H I map, the total surface brightness around the position of the hole. This brightness I_B, which is measured in K km s^{-1}, is converted to volume density according to

$$n_{\rm HI} = 1.823\ 10^{18}\, I_B \cos i/h \sqrt{2\pi}\,. \qquad (1)$$

The factor $\cos i/h \sqrt{2\pi}$ converts the measured column density to volume density. We assume that the distribution of H I as a function of distance from the plane is gaussian with scale height h. We adopt for h a value of 120 pc and for the inclination i a value of 77° (see Paper II for a discussion of these values). It should be noted that the value for $n_{\rm HI}$ derived here corresponds to the volume density at $z=0$. This is in general an upper limit to the volume density of H I surrounding the hole.

The catalogue of H I holes is presented in Table 2. For each hole we list the observed properties:

Column 1: Number of the hole. The holes are numbered according to their position in X (column 2), starting from positions south of the centre of the galaxy.

Columns 2 and 3: Position of the centre of the hole in standard coordinates X and Y with respect to the centre of the galaxy. The same nomenclature is used as in Paper I. Most positions are accurate to 0.′1.

Columns 4 and 5: Position of the centre of the hole in right ascension and declination (1950.0).

Column 6: Radial heliocentric velocity, $V_{\rm Hel}$, at which the hole is most clearly defined, in km s^{-1}. This value is accurate to one channel interval or 4.1 km s^{-1}.

Column 7: Expansion velocity, DV, or half the measured velocity splitting in the case of a Type 3 hole. In the case of a Type 2 hole the negative sign indicates blue-shifted H I. For Type 1 holes no expansion velocity can be measured and the entry is left open. The estimated accuracy to which DV can be given is about 2 km s^{-1}.

Columns 8 and 9: Full width at half depth, FWHMI and FWHMA, measured in parsec along the minor and major axes of the hole, not yet corrected for the size of the beam. The accuracy is about 20–30 pc.

Column 10: Position angle ψ of the major axis of the hole. This position angle is measured in degrees and counter-clockwise with respect to the north declination axis.

Columns 11 and 12: Brightness temperature, INT, of the ambient H I in the channel map at $V_{\rm Hel}$ in Kelvin and the contrast of the hole with respect to its surroundings. The contrast is defined as CONTR = (INT-I$_{50}$)/INT, where I$_{50}$ is the brightness temperature of the H I at half depth, as determined on the basis of the cross-cuts through the channel map.

Column 13: Quality, Q, of the hole.

Column 14: Type, T, of the hole.

Column 15: Class, C, of the hole.
"*c*": complete hole; "*p*": partial hole.

Column 16: Remarks.

The examples shown in Figs. 1–4 illustrate how we classified the holes and how we derived some of the observed properties. Figure 1 gives a set of pictures for H I hole 97. It is a high quality hole ($Q=3$) of type $T=1$. H I is deficient over the full velocity range. This is reflected in the crosscuts made through the integrated H I map which show a run of H I total intensity as a function of position along the cross-cut similar to the cuts made through the channel map at $V_{\rm Hel} = -226.5$ km s^{-1}. Examples of type $T=2$ holes are given in Fig. 2 (hole 66) and Fig. 3 (hole 115). Hole 66 shows a complete inner shell with a diameter of about 500 pc and an incomplete outer shell of about 1000 pc diameter. This hole is one of the few cases in which we can actually see H I shells surrounding the empty inner region. The mean velocity of the H I in the position velocity cuts is seen shifted over about 20 km s^{-1}. Hole 115 (Fig. 3) is also a type $T=2$ hole. The expansion velocity, DV, is about 12 km s^{-1}. Lastly Fig. 4 shows a type $T=3$ hole (hole 48). This hole has a good contrast and has been given a quality rating of $Q=2$. The expansion velocity deduced for this hole is about 14 km s^{-1}.

From the above results we can derive the following set of properties of H I holes. These are listed in Table 3.

Column 1: Number of the hole.

Columns 2 and 3: Position of the hole in polar coordinates in the plane of M 31 with R measured in kpc. The angle θ is measured in degrees, and counter-clockwise with respect to the north major axis of M 31.

Columns 4 and 5: Full width at half depth along the minor and major axis of the hole, given in parsec, after deconvolution for the beam of the observing instrument according to the formulae given by Wild (1970).

Column 6: Position angle of the hole after beam deconvolution. The position angle is measured in degrees and counter-clockwise with respect to the north declination axis.

Columns 7 and 8: Effective diameter of the hole in parsec, defined as the geometric mean of the dimensions of the hole listed in columns 4 and 5, i.e. DIAM = (MINOR × MAJOR)$^{1/2}$, and the axial ratio of the hole defined as RATIO = MINOR/MAJOR. In the case of an unresolved hole the entry for DIAM is left open, and the ratio is 0.0.

Column 9: Volume density, $n_{\rm HI}$, of the H I surrounding the hole estimated, as described above, on the basis of the intensity in the integrated H I map and transformed to atoms cm^{-3} according to formula (1).

Column 10: Kinematic age of the hole in units of 10^6 yr defined as AGE = DIAM/(2 × DV). This age estimate represents an upper limit to the age of a hole. If the evolution of a hole follows that of an expanding shell of swept-up interstellar material in the snowplough phase as described by Weaver et al. (1977; see also Bruhweiler et al., 1980), the age as listed in the table should be reduced to 60 % of its value.

Table 2. Observed properties of H I holes

Name	X (′)	Y (′)	α_{1950} h m s	δ_{1950} ° ′ ″	V_{Hel} (km s^{-1})	DV (km s^{-1})	FWHMI (pc)	FWHMA (pc)	Ψ (°)	Int (K)	Contr	Q	T	C	Remarks
1	53.3 S	8.1 E	0 37 42.7	40 12 33	−506.8	18.6	220	400	0	22.0	0.50	1	3	*p*	
2	52.1 S	3.4 E	0 37 26.7	40 16 20	−552.1	8.2	160	340	158	44.5	0.31	1	3	*p*	
3	49.2 S	12.1 E	0 38 12.6	40 13 24	−486.2	16.5	220	300	0	24.5	0.41	2	2	*c*	
4	48.4 S	9.4 E	0 38 3.8	40 15 41	−477.9	14.4	160	200	0	30.5	0.49	2	3	*c*	
5	48.0 S	5.7 E	0 37 49.6	40 18 12	−560.4	14.4	240	500	0	30.0	0.47	2	3	*c*	
6	47.2 S	4.2 E	0 37 46.0	40 19 43	−572.8	24.7	640	640	0	36.5	0.41	1	2	*c*	
7	46.3 S	13.1 W	0 36 36.7	40 30 57	−457.3		260	400	0	27.0	0.37	1	1	*p*	
8	45.6 S	8.7 E	0 38 9.9	40 18 15	−519.2	−12.4	680	680	0	28.0	0.61	1	2	*p*	
9	45.6 S	13.8 E	0 38 31.1	40 15 14	−477.9		80	140	0	12.0	0.58	1	1	*c*	
10	44.5 S	14.3 E	0 38 36.3	40 15 45	−465.6	8.2	440	440	0	20.5	0.24	1	3	*c*	
11	43.0 S	13.5 W	0 36 45.4	40 33 47	−449.1		260	440	0	24.5	0.29	1	1	*c*	
12	41.7 S	1.5 W	0 37 39.6	40 27 37	−576.9	16.5	100	180	157	17.0	0.59	1	2	*c*	
13	41.3 S	9.2 E	0 38 25.6	40 21 21	−465.6	−12.4	140	280	152	14.5	0.34	1	2	*p*	
14	41.0 S	13.4 E	0 38 44.2	40 19 5	−428.5	−12.4	200	240	0	20.5	0.44	1	2	*p*	
15	39.7 S	15.4 W	0 36 47.9	40 37 36	−445.0		220	360	22	14.0	0.43	1	1	*p*	
16	39.7 S	1.4 W	0 37 46.6	40 29 10	−564.5		420	900	149	25.0	0.40	3	1	*c*	
17	39.3 S	12.5 W	0 37 1.2	40 36 8	−445.0	20.6	300	500	42	34.0	0.41	2	2	*c*	
18	39.3 S	7.7 E	0 38 25.6	40 23 54	−490.3		220	360	53	45.0	0.27	1	1	*c*	
19	38.2 S	8.7 E	0 38 33.5	40 24 10	−469.7	−12.4	560	560	0	35.0	0.49	2	2	*p*	
20	37.9 S	9.5 E	0 38 37.9	40 23 56	−457.3	24.7	500	660	167	14.0	0.50	2	3	*c*	
21	37.7 S	12.2 E	0 38 49.4	40 22 25	−432.6	8.2	120	200	0	34.5	0.32	1	2	*c*	
22	37.5 S	2.2 E	0 38 8.7	40 28 42	−539.8	−12.4	100	200	0	36.5	0.41	3	2	*c*	
23	37.2 S	13.1 W	0 37 5.5	40 38 11	−445.0	12.4	220	320	27	18.0	0.39	1	2	*p*	
24	34.6 S	3.2 W	0 37 55.3	40 34 16	−560.4	8.2	420	660	0	27.0	0.26	1	2	*c*	
25	34.5 S	11.8 E	0 38 58.2	40 25 14	−445.0	20.6	300	480	0	12.5	0.32	1	2	*p*	
26	33.5 S	3.9 W	0 37 56.1	40 35 33	−552.1	14.4	220	280	0	30.5	0.33	2	3	*c*	Blend of two holes
27	33.1 S	15.6 W	0 37 8.0	40 43 0	−424.3		200	220	0	21.0	0.24	1	1	*p*	
28	31.0 S	10.0 E	0 39 1.7	40 29 4	−440.8	12.4	120	140	0	37.5	0.29	1	3	*c*	
29	29.9 S	10.6 E	0 39 7.9	40 29 35	−432.6	12.4	160	160	0	29.0	0.38	1	3	*c*	
30	27.9 S	10.7 W	0 37 45.2	40 44 9	−424.3	14.4	100	160	0	8.5	0.59	1	3	*c*	
31	26.8 S	16.7 W	0 37 23.7	40 48 38	−362.5	12.4	80	160	31	14.0	0.57	1	3	*p*	
32	23.8 S	14.1 W	0 37 44.1	40 49 27	−391.4	8.2	180	180	0	25.5	0.35	1	2	*c*	
33	23.6 S	12.5 E	0 39 36.1	40 33 25	−395.5	14.4	120	140	0	23.0	0.43	1	3	*c*	
34	22.8 S	4.8 E	0 39 6.9	40 38 44	−482.1		220	360	40	22.5	0.49	1	1	*p*	
35	21.7 S	11.2 E	0 39 37.0	40 35 42	−383.1	18.6	160	280	0	19.5	0.41	1	3	*p*	
36	18.6 S	12.3 E	0 39 51.1	40 37 29	−379.0	8.2	260	420	122	28.5	0.46	2	2	*c*	
37	17.4 S	8.9 W	0 38 26.7	40 51 20	−424.3	14.4	100	220	0	27.0	0.33	1	3	*c*	
38	16.4 S	8.1 E	0 39 41.4	40 41 48	−436.7	12.4	100	120	0	17.0	0.41	1	3	*c*	
39	16.3 S	8.3 W	0 38 32.9	40 51 51	−436.7	10.3	160	280	39	23.0	0.43	1	3	*c*	
40	15.9 S	12.0 E	0 39 59.1	40 39 46	−366.6	12.4	280	520	45	24.0	0.50	2	3	*c*	
41	15.3 S	8.2 W	0 38 36.5	40 52 37	−428.5	12.4	140	320	44	26.5	0.34	1	3	*c*	
42	11.2 S	9.5 W	0 38 44.4	40 56 40	−403.7	14.4	100	120	0	43.0	0.28	1	3	*c*	
43	8.8 S	9.7 E	0 40 12.4	40 46 52	−387.3	8.2	260	360	132	27.5	0.33	1	2	*p*	
44	8.4 S	8.1 E	0 40 7.1	40 48 8	−354.3		100	240	22	16.0	0.50	1	1	*c*	
45	8.3 S	10.6 E	0 40 17.7	40 46 37	−354.3	20.6	500	800	37	50.0	0.44	2	3	*c*	
46	6.4 S	14.4 E	0 40 39.9	40 45 50	−354.3	20.6	560	820	30	24.0	0.50	1	2	*p*	
47	6.1 S	12.8 W	0 38 46.9	41 2 43	−313.0	− 8.2	200	380	75	22.5	0.31	1	2	*c*	Blend of three holes
48	5.5 S	11.0 E	0 40 28.4	40 48 38	−337.8	14.4	220	360	0	29.5	0.31	2	3	*c*	
49	5.1 S	9.9 W	0 39 2.1	41 1 44	−354.3	16.5	160	260	0	27.0	0.41	2	3	*c*	As 50, different V_{Hel}
50	5.0 S	10.2 W	0 39 1.2	41 1 59	−383.1	12.4	100	120	0	20.5	0.39	1	2	*c*	As 49, different V_{Hel}
51	3.5 S	14.4 W	0 38 48.7	41 5 44	−308.9	− 8.2	240	360	0	25.0	0.32	2	2	*c*	
52	3.1 S	12.7 W	0 38 56.7	41 4 60	−337.8	24.7	480	600	38	17.0	0.41	1	2	*p*	
53	1.4 S	11.7 E	0 40 44.4	40 51 24	−313.0	10.3	160	240	0	41.0	0.32	2	3	*c*	
54	0.6 S	10.4 E	0 40 41.8	40 52 55	−341.9	12.4	500	900	51	30.0	0.43	1	2	*p*	
55	1.5 N	10.0 W	0 39 23.4	41 7 2	−292.4	14.4	160	240	0	18.5	0.27	1	3	*c*	
56	1.8 N	10.9 E	0 40 51.6	40 54 25	−329.5	8.2	140	140	0	14.5	0.48	1	2	*c*	
57	1.8 N	12.6 E	0 40 58.7	40 53 24	−296.6	10.3	160	240	57	32.0	0.22	1	3	*c*	
58	2.5 N	15.6 W	0 39 2.9	41 11 17	−292.4		140	240	127	28.0	0.25	1	1	*c*	
59	2.8 N	9.3 E	0 40 48.0	40 56 12	−329.5	12.4	140	200	0	18.5	0.49	1	2	*c*	
60	4.2 N	8.2 W	0 39 39.5	41 8 3	−296.6	16.5	480	480	0	21.5	0.37	2	2	*p*	
61	5.6 N	9.6 E	0 40 58.7	40 58 12	−280.1	−12.4	260	400	0	26.0	0.23	2	2	*c*	
62	6.1 N	10.3 E	0 41 3.2	40 58 12	−300.7	20.6	620	620	0	35.5	0.37	2	2	*c*	
63	7.6 N	11.9 E	0 41 14.8	40 58 26	−284.2	8.2	380	580	139	45.0	0.27	1	2	*c*	
64	8.9 N	13.6 E	0 41 26.3	40 58 25	−271.8	10.3	160	220	104	33.0	0.18	1	3	*c*	Blend of two holes
65	11.6 N	8.8 E	0 41 14.9	41 3 28	−275.9	12.4	160	260	0	24.5	0.24	1	2	*c*	
66	12.8 N	10.4 E	0 41 25.6	41 3 27	−271.8	20.6	500	560	0	31.0	0.35	2	2	*c*	Concentric shell 5′.0
67	13.0 N	13.2 W	0 39 47.5	41 18 5	−255.3	12.4	140	240	50	29.5	0.27	1	2	*c*	Blend of two holes
68	14.7 N	14.3 W	0 39 48.4	41 20 5	−263.6	12.4	220	280	0	23.5	0.38	3	3	*c*	See also 69
69	14.7 N	14.3 W	0 39 48.4	41 20 5	−263.6		1000	1400	39	23.5	0.38	3	1	*p*	Concentric with 68
70	16.0 N	8.8 E	0 41 29.2	41 6 58	−214.1	− 8.2	120	200	0	13.5	0.74	1	2	*c*	
71	16.0 N	9.6 E	0 41 32.8	41 6 27	−247.1	12.4	380	620	0	39.0	0.36	2	3	*c*	
72	17.6 N	10.9 W	0 40 11.6	41 20 20	−218.2	18.6	120	260	67	26.0	0.35	1	3	*c*	

Table 2 (continued)

Name	X (′)	Y (′)	α_{1950} h m s	δ_{1950} ° ′ ″	V_{Hel} (km s^{-1})	DV (km s^{-1})	FWHMI (pc)	FWHMA (pc)	Ψ (°)	Int (K)	Contr	Q	T	C	Remarks
73	19.0 N	12.9 W	0 40 8.1	41 22 36	−226.5	−12.4	80	120	0	31.5	0.22	1	2	*c*	
74	19.0 N	10.3 W	0 40 18.8	41 21 5	−218.2	18.6	140	160	0	24.0	0.38	1	3	*c*	
75	19.6 N	11.2 W	0 40 17.0	41 22 5	−234.7	12.4	140	280	67	32.5	0.28	1	2	*c*	
76	20.7 N	10.7 E	0 41 52.5	41 9 26	−201.8		180	300	32	49.0	0.18	1	1	*c*	Close to 79 and 77
77	21.2 N	12.2 E	0 42 0.5	41 8 54	−226.5	20.6	220	220	0	24.0	0.33	2	2	*c*	Close to 76 and 79
78	21.8 N	13.3 W	0 40 15.2	41 25 5	−210.0	−16.5	120	280	44	19.0	0.21	1	2	*c*	
79	21.9 N	11.5 E	0 41 59.6	41 9 55	−201.8		180	180	0	50.5	0.24	1	1	*c*	Close to 76 and 77
80	22.5 N	9.5 W	0 40 34.0	41 23 20	−193.5	20.6	280	360	0	20.0	0.40	1	3	*c*	
81	22.8 N	15.6 W	0 40 9.0	41 27 20	−222.4	−16.5	140	240	142	25.5	0.35	1	2	*c*	
82	23.1 N	11.6 W	0 40 26.9	41 25 5	−226.5	16.5	360	460	0	24.0	0.33	1	3	*p*	
83	23.4 N	8.4 W	0 40 41.2	41 23 20	−214.1	10.3	80	120	0	18.0	0.22	1	3	*c*	
84	24.6 N	17.4 W	0 40 7.2	41 29 50	−238.8	10.3	180	180	0	26.5	0.42	1	3	*c*	
85	24.7 N	8.8 N	0 40 43.9	41 24 34	−226.5	8.2	180	240	0	17.5	0.40	1	2	*c*	
86	25.8 N	9.4 W	0 40 44.8	41 25 49	−197.6	−12.4	140	300	137	40.0	0.27	2	2	*p*	
87	25.8 N	9.9 E	0 42 6.0	41 13 55	−205.9		200	460	26	58.0	0.24	1	1	*c*	
88	25.9 N	10.0 W	0 40 43.0	41 26 19	−201.8	− 8.2	100	180	35	50.5	0.28	1	2	*c*	
89	27.0 N	9.1 W	0 40 50.2	41 26 34	−193.5	−28.9	80	140	0	38.0	0.24	1	2	*c*	
90	27.2 N	2.7 E	0 41 40.2	41 19 29	− 61.6	−12.4	260	260	0	8.5	0.47	1	2	*p*	
91	27.3 N	9.8 E	0 42 10.5	41 15 9	−172.9	16.5	180	500	152	29.0	0.21	2	2	*p*	
92	27.3 N	10.2 W	0 40 46.6	41 27 34	−177.0	− 4.1	140	140	0	15.5	0.32	1	2	*p*	
93	27.6 N	12.3 E	0 42 22.1	41 13 52	−181.1	− 8.2	160	300	35	18.5	0.32	1	2	*c*	
94	27.7 N	8.4 E	0 42 6.1	41 16 25	−201.8		240	240	0	27.0	0.22	1	1	*p*	
95	27.9 N	22.1 W	0 39 58.2	41 35 19	−238.8	12.4	140	300	37	19.0	0.37	1	2	*c*	
96	28.4 N	9.3 E	0 42 12.3	41 16 24	−144.0	−16.5	220	240	0	25.0	0.48	2	2	*c*	
97	28.9 N	15.9 W	0 40 27.8	41 32 19	−226.5		240	380	132	17.0	0.29	3	1	*c*	
98	29.6 N	17.1 W	0 40 25.1	41 33 34	−218.2	16.5	260	500	164	14.0	0.29	1	3	*p*	
99	29.9 N	12.0 E	0 42 28.4	41 15 51	−177.0	−12.4	180	360	0	20.0	0.25	1	2	*c*	
100	30.4 N	8.6 E	0 42 16.0	41 18 24	−197.6	12.4	220	380	0	14.0	0.14	1	2	*p*	
101	30.7 N	11.9 E	0 42 30.2	41 16 36	−152.3		100	160	154	31.5	0.35	2	1	*c*	
102	30.9 N	10.4 W	0 40 57.4	41 30 33	−197.6	16.5	240	340	0	33.5	0.27	1	2	*c*	
103	31.0 N	12.8 W	0 40 47.6	41 32 4	−214.1	12.4	420	420	0	18.5	0.38	1	3	*c*	
104	31.0 N	17.3 W	0 40 28.7	41 34 49	−243.0	12.4	100	140	0	20.0	0.25	1	2	*c*	
105	31.3 N	14.5 W	0 40 41.3	41 33 19	−189.4	− 8.2	80	160	0	14.0	0.29	1	2	*p*	
106	31.9 N	16.9 W	0 40 33.2	41 35 19	−230.6	− 8.2	280	460	0	25.5	0.31	2	2	*c*	
107	31.9 N	8.1 E	0 42 18.7	41 19 53	−177.0	10.3	220	440	23	31.5	0.38	2	3	*c*	
108	32.3 N	9.8 W	0 41 4.6	41 31 17	−193.5	16.5	100	160	0	27.5	0.33	1	2	*c*	
109	32.5 N	11.3 W	0 40 59.3	41 32 18	−177.0	12.4	140	200	39	37.5	0.29	1	3	*c*	
110	33.0 N	8.3 E	0 42 23.2	41 20 38	−139.9	16.5	160	180	0	30.0	0.33	2	2	*c*	
111	33.5 N	19.4 W	0 40 27.9	41 38 3	−226.5		180	200	0	14.5	0.34	1	1	*c*	
112	33.8 N	8.0 W	0 41 17.2	41 31 16	−148.2		140	320	52	34.0	0.32	1	1	*c*	
113	33.9 N	9.8 E	0 42 32.2	41 20 21	−168.8	16.5	140	160	0	28.0	0.25	2	2	*c*	
114	34.0 N	17.5 W	0 40 37.8	41 37 18	−218.2	− 8.2	600	800	0	12.0	0.42	3	2	*p*	
115	34.5 N	10.2 E	0 42 35.7	41 20 36	−177.0	12.4	360	360	0	30.0	0.33	3	2	*p*	
116	34.8 N	7.4 E	0 42 25.1	41 22 38	−127.5	12.4	200	200	0	35.0	0.29	2	2	*c*	
117	35.2 N	10.3 E	0 42 38.5	41 21 5	−123.4	−16.5	120	200	138	14.0	0.36	1	2	*p*	
118	37.4 N	8.2 W	0 41 28.0	41 34 15	−127.5	− 8.2	120	200	0	18.0	0.44	1	2	*c*	
119	37.8 N	7.3 W	0 41 33.4	41 33 59	−123.4	− 8.2	100	160	0	10.5	0.29	1	2	*c*	
120	39.4 N	17.8 W	0 40 54.0	41 41 46	−214.1		460	540	45	13.0	0.31	3	1	*p*	
121	39.5 N	6.5 E	0 42 36.9	41 26 50	−115.2	8.2	160	300	0	28.0	0.21	1	2	*c*	
122	40.4 N	8.4 W	0 41 37.1	41 36 43	−139.9	16.5	220	220	0	27.0	0.37	2	2	*c*	
123	40.6 N	8.0 E	0 42 46.8	41 26 48	−115.2	10.3	240	320	0	29.0	0.34	1	3	*c*	
124	40.9 N	14.3 W	0 41 13.8	41 40 45	−168.8	−12.4	160	220	0	18.5	0.38	1	2	*p*	
125	41.4 N	17.3 W	0 41 3.0	41 42 60	−210.0	12.4	220	360	54	15.0	0.27	1	2	*c*	
126	41.9 N	7.2 W	0 41 47.0	41 37 12	− 98.7	−12.4	160	260	124	25.5	0.31	2	2	*p*	
127	42.1 N	9.1 E	0 42 56.6	41 27 16	−144.0	20.6	220	420	0	29.5	0.34	1	2	*c*	
128	43.5 N	7.2 W	0 41 52.4	41 38 26	− 82.2	− 8.2	100	160	0	7.5	0.40	1	2	*p*	
129	43.5 N	6.4 E	0 42 49.6	41 30 2	− 82.2	−12.4	120	200	40	28.0	0.36	2	2	*c*	
130	44.8 N	3.8 W	0 42 11.3	41 37 23	− 69.8	−20.6	680	680	0	16.5	0.48	3	2	*p*	
131	45.6 N	17.1 W	0 41 17.5	41 46 12	−197.6		140	140	0	22.5	0.40	1	1	*c*	
132	45.6 N	1.8 E	0 42 37.2	41 34 34	− 61.6	−12.4	480	480	0	42.0	0.45	1	2	*p*	
133	46.2 N	11.4 W	0 41 43.5	41 43 10	−148.2	8.2	200	260	100	21.0	0.33	1	3	*c*	
134	46.2 N	2.6 E	0 42 42.6	41 34 33	− 69.8	− 8.2	100	160	32	47.0	0.19	1	2	*c*	
135	47.0 N	6.5 E	0 43 1.4	41 32 44	− 82.2		80	240	170	30.0	0.17	1	1	*c*	
136	47.9 N	14.9 W	0 41 34.6	41 46 40	−185.3		240	340	45	26.5	0.34	1	1	*c*	
137	48.1 N	0.5 E	0 42 40.0	41 37 18	−57.5		80	140	0	42.5	0.14	1	1	*c*	
138	49.3 N	2.9 E	0 42 54.4	41 36 45	− 74.0	8.2	180	240	0	66.0	0.30	1	2	*c*	
139	50.7 N	1.8 W	0 42 39.3	41 40 47	− 61.6	18.6	240	420	0	44.0	0.36	1	3	*c*	
140	51.3 N	6.4 W	0 42 21.4	41 44 4	− 61.6	−12.4	120	200	0	33.0	0.45	1	2	*c*	
141	52.8 N	3.2 W	0 42 40.3	41 43 16	− 57.5		140	280	130	45.5	0.29	1	1	*c*	

Table 3. Derived properties of H I holes

Name	R (kpc)	θ (°)	Minor (pc)	Major (pc)	P.A. (°)	Diam. (pc)	Ratio	n_{HI} (at cm^{-3})	Age (10^6 yr)	Mass ($10^4 M_\odot$)	Energy (10^{50} erg)
1	12.85	146.0	200	380	0	276	0.53	0.45	7.3	12.2	61.2
2	10.85	164.0	140	320	156	212	0.44	0.45	12.6	5.5	8.6
3	14.57	132.4	200	280	0	237	0.71	0.44	7.0	7.6	31.5
4	12.77	139.3	140	160	0	150	0.87	0.66	5.1	2.9	9.9
5	10.85	152.2	220	480	0	325	0.46	0.49	11.0	22.0	79.9
6	10.16	158.3	620	640	90	630	0.97	0.66	12.5	214.5	1858.7
7	14.87	231.5	240	380	0	302	0.63	0.35		12.6	19.1
8	11.98	139.6	660	680	90	670	0.97	0.57	26.5	223.6	727.1
9	15.27	126.6	0	80	0		0.00	0.27			
10	15.49	125.1	420	440	90	430	0.95	0.25	25.5	25.4	40.2
11	14.76	234.3	240	420	0	317	0.57	0.37		15.4	23.6
12	8.45	189.4	40	140	148	75	0.29	0.33	2.2	0.2	0.6
13	11.65	135.2	100	260	149	161	0.38	1.06	6.4	5.8	17.0
14	14.47	124.5	180	200	0	190	0.90	0.40	7.5	3.5	9.4
15	15.84	239.9	200	340	24	261	0.59	0.27		6.1	8.8
16	8.03	189.1	400	900	149	600	0.44	0.37		103.8	171.8
17	13.63	234.7	280	480	43	367	0.58	0.46	8.7	29.3	176.5
18	10.40	139.1	200	340	56	261	0.59	0.64		14.6	23.3
19	10.87	134.6	540	560	90	550	0.96	0.62	21.7	133.2	426.7
20	11.35	131.9	500	640	166	566	0.78	0.62	11.2	145.0	1230.0
21	13.19	124.9	80	160	0	113	0.50	0.51	6.7	1.0	1.4
22	7.74	165.4	60	160	0	98	0.37	0.52	3.9	0.6	1.6
23	13.82	237.4	200	300	31	245	0.67	0.50	9.7	9.6	27.2
24	7.49	202.5	420	640	0	518	0.66	0.42	30.7	76.5	131.9
25	12.54	123.4	280	460	0	359	0.61	0.28	8.5	16.9	95.9
26	7.53	207.2	200	260	0	228	0.77	0.47	7.7	7.2	24.9
27	15.41	244.6	180	180	0	180	1.00	0.27		2.0	2.8
28	10.81	125.0	80	80	0	80	1.00	0.62	3.2	0.4	1.0
29	11.15	122.5	100	140	90	118	0.71	0.44	4.7	4.9	2.4
30	11.06	239.7	60	100	0	77	0.60	0.41	2.6	0.2	0.7
31	15.78	250.1	0	120	43		0.00	0.15			
32	13.44	249.2	140	160	90	150	0.87	0.35	8.9	1.5	2.2
33	12.06	113.0	80	80	0	80	1.00	0.42	2.7	0.3	0.8
34	6.27	136.6	200	340	43	261	0.59	0.37		8.5	12.8
35	10.87	113.5	140	260	0	191	0.54	0.39	5.0	3.5	16.5
36	11.51	108.9	240	400	120	310	0.60	0.27	18.4	10.2	15.6
37	8.62	246.1	60	180	0	104	0.33	0.69	3.5	1.0	3.3
38	7.94	114.3	0	60	90		0.00	0.37			
39	8.04	246.1	120	260	43	177	0.46	0.53	8.4	3.8	8.0
40	11.17	106.5	260	500	46	361	0.52	0.42	14.3	25.7	74.9
41	7.90	247.2	100	300	47	173	0.33	0.42	6.8	2.9	7.6
42	8.71	255.1	0	60	90		0.00	0.81			
43	8.79	101.5	240	340	128	286	0.71	0.71	16.9	21.3	36.4
44	7.41	103.0	40	220	26	94	0.18	0.48		0.5	0.7
45	9.61	100.0	500	800	38	632	0.63	0.74	15.0	243.1	1655.4
46	12.89	95.7	560	820	31	678	0.68	0.42	16.1	170.9	1097.0
47	11.43	263.9	160	380	76	247	0.42	0.46	14.6	8.9	14.2
48	9.84	96.4	200	340	0	261	0.59	0.85	8.8	19.5	73.5
49	8.88	263.4	140	240	0	183	0.58	0.69	5.4	5.5	23.4
50	9.12	263.7	0	60	90		0.00	0.69			
51	12.80	266.9	220	340	0	273	0.65	0.53	16.2	14.0	23.0
52	11.32	266.8	460	600	40	525	0.77	0.46	10.4	86.3	700.0
53	10.40	91.6	140	200	0	167	0.70	0.78	7.9	4.7	10.4
54	9.21	90.7	480	900	51	657	0.53	0.78	26.0	285.9	961.8
55	8.87	272.0	140	200	0	167	0.70	0.66	5.7	4.0	14.0
56	9.69	87.9	80	120	90	98	0.67	0.78	5.8	0.9	1.4

Table 3 (continued)

Name	R (kpc)	θ (°)	Minor (pc)	Major (pc)	P.A. (°)	Diam. (pc)	Ratio	n_{HI} (at cm^{-3})	Age (10^6 yr)	Mass ($10^4\,M_\odot$)	Energy (10^{50} erg)
57	11.19	88.2	120	220	63	162	0.55	0.73	7.7	4.1	8.9
58	13.91	272.1	80	220	122	133	0.36	0.32		1.0	1.3
59	8.27	86.2	120	160	0	139	0.75	0.70	5.5	2.4	6.6
60	7.34	276.6	460	480	90	470	0.96	0.28	13.9	38.0	162.6
61	8.64	82.6	240	380	0	302	0.63	0.50	11.9	18.0	52.3
62	9.25	82.4	600	620	90	610	0.97	0.67	14.5	197.3	1321.5
63	10.67	81.8	360	580	138	457	0.62	0.74	27.1	91.7	166.5
64	12.24	81.6	100	200	100	141	0.50	0.69	6.7	2.5	5.4
65	8.16	73.5	140	240	0	183	0.58	0.65	7.2	5.2	14.7
66	9.60	74.5	500	540	0	520	0.93	0.85	12.3	154.1	1041.3
67	11.99	282.6	100	220	56	148	0.45	0.48	5.9	2.0	5.4
68	13.01	283.1	200	260	0	228	0.77	0.31	9.0	4.7	12.6
69	13.01	283.1	1000	1400	39	1183	0.71	0.31		663.3	1165.2
70	8.43	67.7	80	160	0	113	0.50	0.65	6.7	1.2	1.9
71	9.13	69.5	380	600	0	477	0.63	0.68	18.9	95.9	305.6
72	10.35	289.9	40	240	70	98	0.17	0.79	2.6	1.0	4.5
73	12.05	288.4	0	0	0			0.53			
74	9.96	292.5	100	120	90	110	0.83	0.87	2.9	1.5	7.1
75	10.73	291.4	80	260	70	144	0.31	0.69	5.7	2.7	7.4
76	10.38	66.5	160	280	36	212	0.57	1.06		13.0	21.6
77	11.65	68.7	180	200	90	190	0.90	0.83	4.5	7.3	43.9
78	12.63	290.2	60	260	48	125	0.23	0.57	3.7	1.4	5.7
79	11.10	66.8	140	160	90	150	0.87	0.97		4.2	6.6
80	9.55	298.2	260	340	0	297	0.76	0.69	7.1	23.5	144.6
81	14.64	288.2	100	220	136	148	0.45	0.41	4.4	1.7	6.7
82	11.30	294.1	360	440	0	398	0.82	0.58	11.8	47.6	217.9
83	8.81	302.0	0	0	0			0.53			
84	16.26	287.6	140	160	90	150	0.87	0.38	7.1	1.6	3.3
85	9.23	302.3	160	200	0	179	0.80	0.62	10.6	4.6	7.3
86	9.82	301.7	100	280	134	167	0.36	0.66	6.6	4.0	11.3
87	10.23	59.8	180	440	27	281	0.41	1.22		35.2	61.3
88	10.27	300.3	20	140	45	53	0.14	0.73	3.1	0.1	0.2
89	9.69	303.8	0	80	0		0.00	0.83			
90	5.94	23.8	240	240	0	240	1.00	0.25	9.5	4.4	11.5
91	10.31	58.1	160	480	151	277	0.33	1.27	8.2	35.1	168.8
92	10.60	301.1	80	120	90	98	0.67	0.76	11.6	0.9	0.5
93	12.29	63.3	120	280	38	183	0.43	0.73	10.9	5.8	9.5
94	9.30	53.4	200	220	90	210	0.91	0.64		7.6	11.8
95	20.44	285.8	100	280	40	167	0.36	0.18	6.6	1.1	2.6
96	10.07	55.6	200	200	0	200	1.00	1.03	5.9	10.7	48.4
97	15.28	292.3	220	360	129	281	0.61	0.43		12.5	19.2
98	16.29	291.3	240	480	163	339	0.50	0.32	10.1	16.1	67.3
99	12.27	60.8	160	340	0	233	0.47	0.81	9.2	13.4	39.9
100	9.81	51.6	200	360	0	268	0.56	0.60	10.6	15.0	44.0
101	12.20	59.8	40	120	139	69	0.33	0.72		0.3	0.4
102	11.16	303.7	220	320	0	265	0.69	0.76	7.9	18.4	82.7
103	12.98	298.5	400	420	90	410	0.95	0.66	16.2	59.1	184.3
104	16.58	292.0	60	80	0	69	0.75	0.33	2.7	0.1	0.3
105	14.34	295.8	0	100	0		0.00	0.51			
106	16.36	293.0	260	440	0	338	0.59	0.28	20.1	14.2	22.1
107	9.65	48.5	200	420	24	290	0.48	0.62	13.7	19.5	44.8
108	10.88	306.5	60	100	0	77	0.60	0.81	2.3	0.5	1.9
109	11.93	303.0	100	180	50	134	0.56	0.84	5.3	2.6	7.4
110	9.93	48.3	140	140	0	140	1.00	0.82	4.2	2.9	12.3
111	18.51	291.2	160	160	0	160	1.00	0.11		0.6	0.7
112	9.79	313.6	80	300	55	155	0.27	0.90		4.3	6.8

Table 3 (continued)

Name	R	θ	Minor	Major	P.A.	Diam.	Ratio	$n_{\mathrm{H\,I}}$	Age	Mass	Energy
	(kpc)	(°)	(pc)	(pc)	(°)	(pc)		(at cm^{-3})	(10^6 yr)	($10^4\,M_\odot$)	(10^{50} erg)
113	11.06	52.2	100	120	90	110	0.83	1.00	3.2	1.7	7.1
114	16.97	293.6	600	800	0	693	0.75	0.30	41.1	129.4	221.5
115	11.40	52.8	340	360	90	350	0.94	0.85	13.8	47.0	148.3
116	9.57	43.3	160	180	90	170	0.89	0.71	6.7	4.5	12.6
117	11.55	52.5	60	180	129	104	0.33	0.74	3.1	1.1	4.3
118	10.44	315.7	80	160	0	113	0.50	0.78	6.7	1.5	2.3
119	9.93	319.5	60	100	0	77	0.60	0.67	4.6	0.4	0.6
120	17.71	296.4	440	540	48	487	0.81	0.17		25.2	36.9
121	9.79	36.2	140	280	0	198	0.50	0.88	11.7	8.9	14.9
122	11.00	317.2	180	200	90	190	0.90	0.74	5.6	6.6	28.3
123	10.79	41.2	220	300	0	257	0.73	1.02	12.2	22.5	54.2
124	15.11	302.7	140	180	0	159	0.78	0.46	6.3	2.4	6.3
125	17.44	298.3	200	340	57	261	0.59	0.25	10.3	5.7	14.9
126	10.56	322.5	120	240	119	170	0.50	0.65	6.7	4.1	11.6
127	11.71	44.0	200	400	0	283	0.50	0.65	6.7	19.2	116.6
128	10.79	323.7	60	100	0	77	0.60	0.75	4.6	0.5	0.7
129	10.39	33.2	60	180	49	104	0.33	0.80	4.1	1.2	3.1
130	9.58	339.5	660	680	90	670	0.97	0.55	15.9	213.3	1409.9
131	17.74	300.9	80	120	90	98	0.67	0.16		0.2	0.2
132	9.26	9.8	460	480	90	470	0.96	0.37	18.6	49.9	147.4
133	13.73	312.3	160	240	98	196	0.67	0.43	11.6	4.2	6.5
134	9.53	13.9	20	120	47	49	0.17	0.51	2.9	0.1	0.1
135	11.01	31.4	0	200	168		0.00	0.67			
136	16.34	305.9	220	320	49	265	0.69	0.35		8.5	12.8
137	9.63	2.6	0	80	0		0.00	0.60			
138	10.21	14.9	160	200	0	179	0.80	0.80	10.6	5.9	9.6
139	10.27	351.2	220	400	0	297	0.55	0.63	7.8	21.2	111.5
140	11.73	330.9	80	160	0	113	0.50	0.57	4.5	1.1	2.8
141	10.93	345.1	100	260	126	161	0.38	0.60		3.3	4.9

Column 11: Indicative H I mass in units of $10^4\,M_\odot$. We evaluate the mass which might have been present at the position of the hole under the assumption that the hole is entirely empty, that $\frac{\pi}{6}(\mathrm{DIAM})^3$ is the characteristic volume of the hole, and that $n_{\mathrm{H\,I}}$ is the average H I volume density if the hole were not present.

Column 12: Indicative energy needed to produce a hole in units of 10^{50} erg. To facilitate comparisons with the work by Heiles (1979) for the shells in our Galaxy we use the same expression as used by him for the energy deposited in the interstellar medium, i.e.

$$E = 5.3\ 10^{43}\, n_{\mathrm{H\,I}}{}^{1.12}\,(\mathrm{DIAM}/2)^{3.12}\, DV^{1.4}\ \mathrm{erg}. \tag{2}$$

In the case of a Type 1 hole no expansion velocity can be measured, so we take for DV the velocity dispersion of the gas, i.e. 8 km s^{-1} (see Paper II).

The mass estimate listed in the table represents in general an upper limit, due to our choice of $n_{\mathrm{H\,I}}$ for the volume density evacuated through formation of the hole. As a check on the indicative mass we calculated for a few holes the H I mass which might have been present at the position of the hole based on the H I missing from the channel maps and the velocity range over which this H I is absent. These H I masses agreed to within a factor of two with the indicative mass.

3. Descriptive statistics for the H I holes

3.1. General results

The total number of holes which we have found is 141. Figure 5 shows the distribution of these holes in M 31. Each hole in this figure is represented as an ellipse with the dimensions given in Table 2, i.e. not corrected for the size of the beam. The H I holes are predominantly found in a ring at about 10 kpc from the centre and are, necessarily, closely correlated with the H I distribution. Due to its high inclination, the spiral pattern of M 31, if present, is not at all easy to trace. Various authors have attempted to identify the location and sense of winding of the spiral arms in M 31, but these studies have not yet provided a generally accepted spiral pattern. Also the distribution of the H I holes, which are relatively young objects of about 10^6–10^7 yr (see Table 3) and thus expected to be closely correlated with spiral arms, does not clarify this picture. Looking at Fig. 5, it is not possible to distinguish between a two armed trailing spiral pattern as proposed by Arp (1964) and also favoured by Hodge (1979) from the distribution of open clusters, and a one armed leading spiral as discussed by Simien et al. (1978) from the distribution of H II regions listed by Pellet et al. (1978).

For the interpretation of the data on holes it is important to realize that our catalogue is not complete. Although the search was

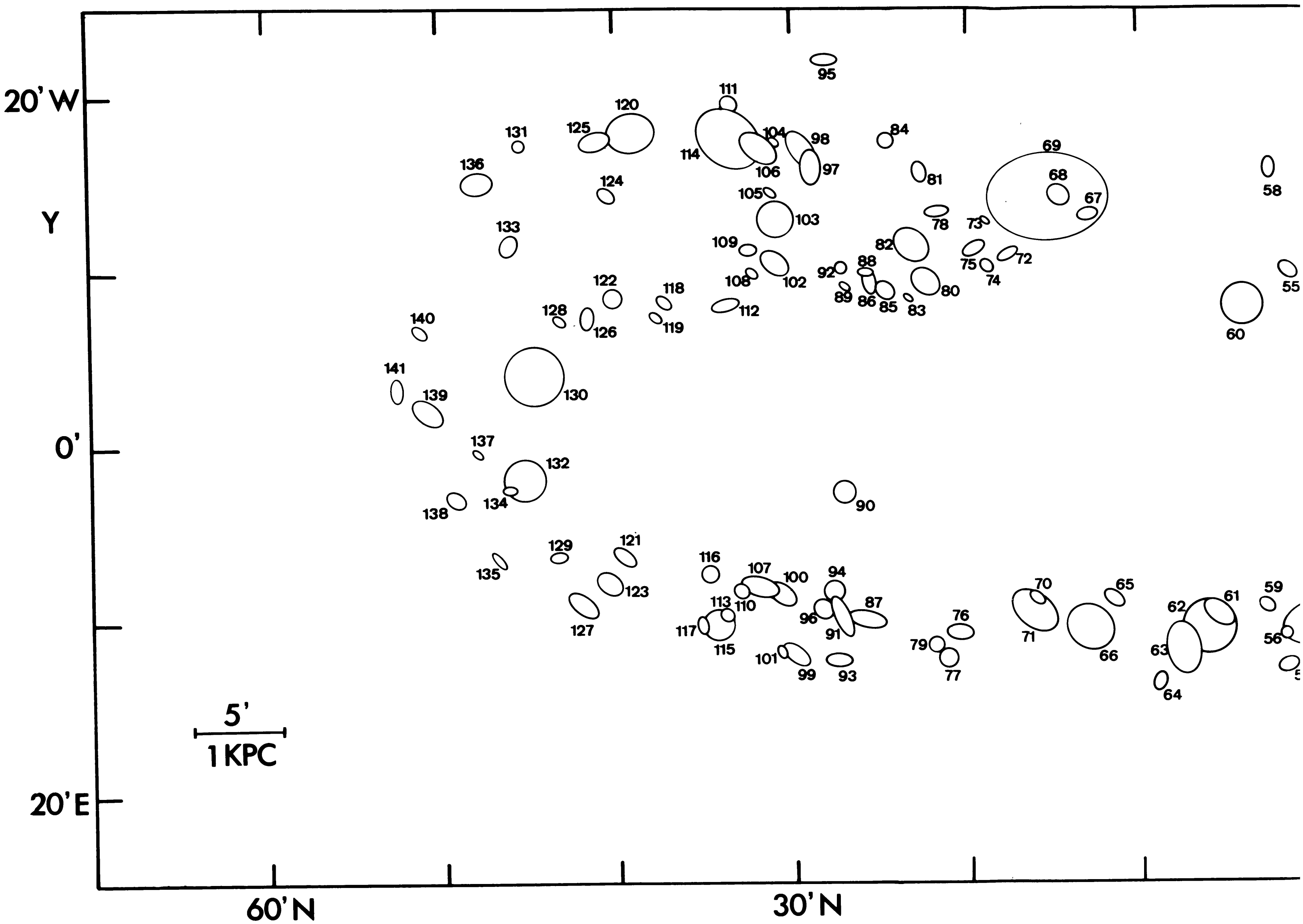

Fig. 5. Distribution of H I holes in M 31. Each hole is indicated as an ellipse with the dimensions as listed in Table 2, i.e. uncorrected for the beam of the observing instrument

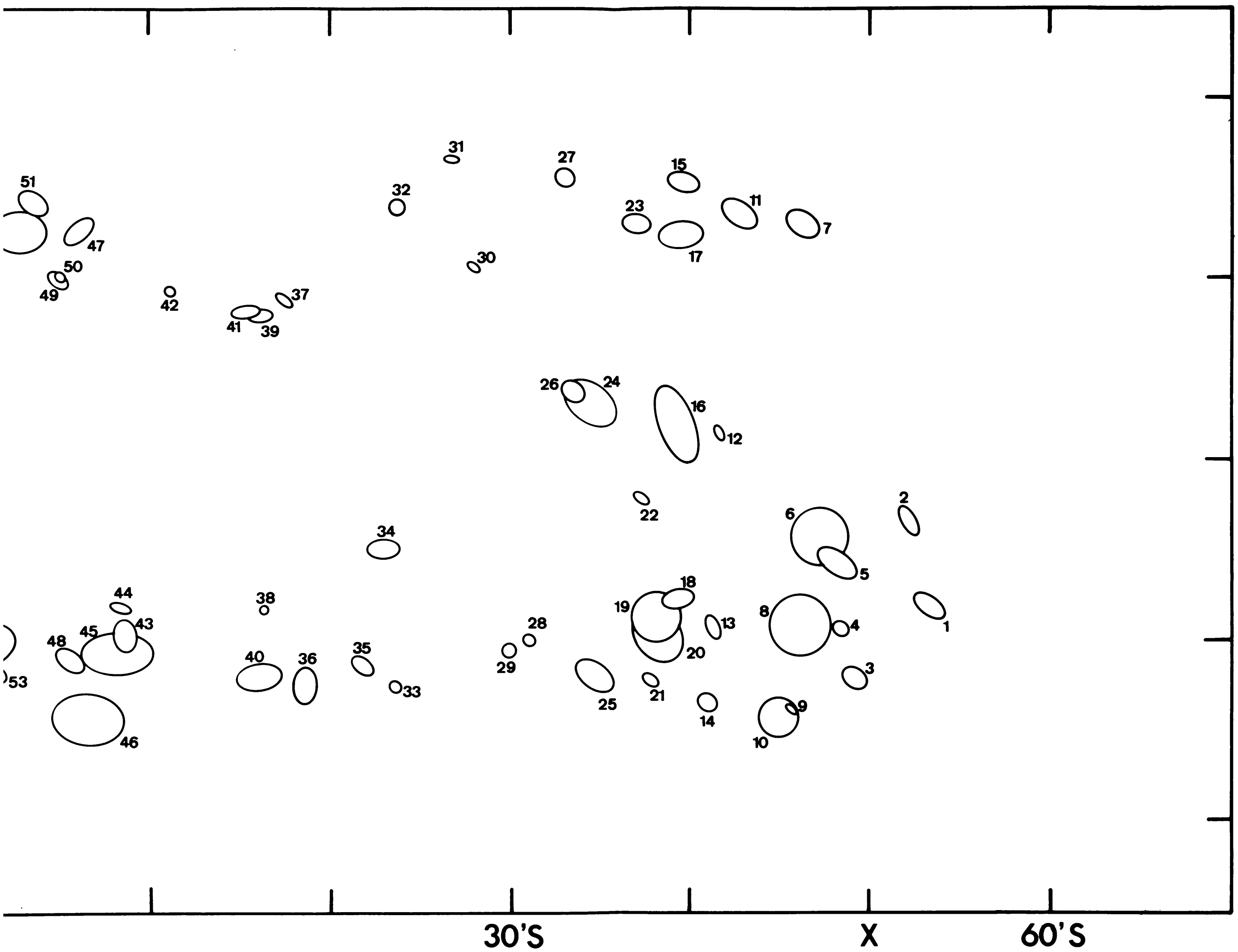
31
27
15
51
32
23
11
7
47
17
30
50
49
42
37
41
39
26
24
16
12
22
2
6
34
5
18
44
38
19
13
8
4
1
43
45
48
28
40
36
35
20
3
29
53
33
25
21
14
9
46
10
30'S
X
60'S

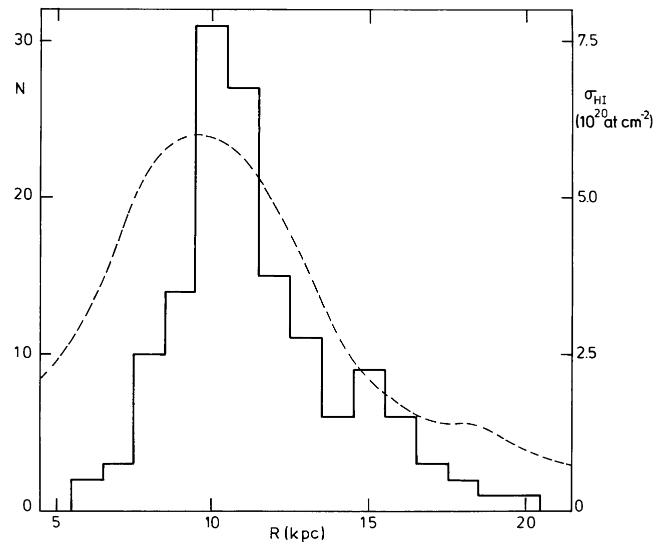

Fig. 6. Radial distribution of H I holes. The dashed line shows the average H I surface density, σ_{HI}, as a function of radius

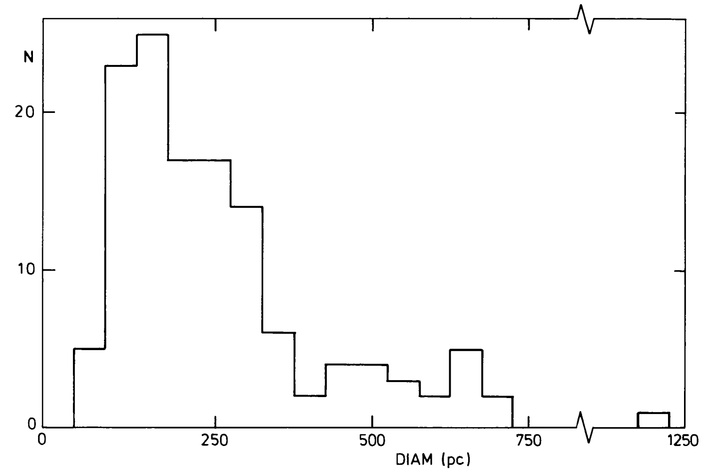

Fig. 8. Size distribution of the H I holes

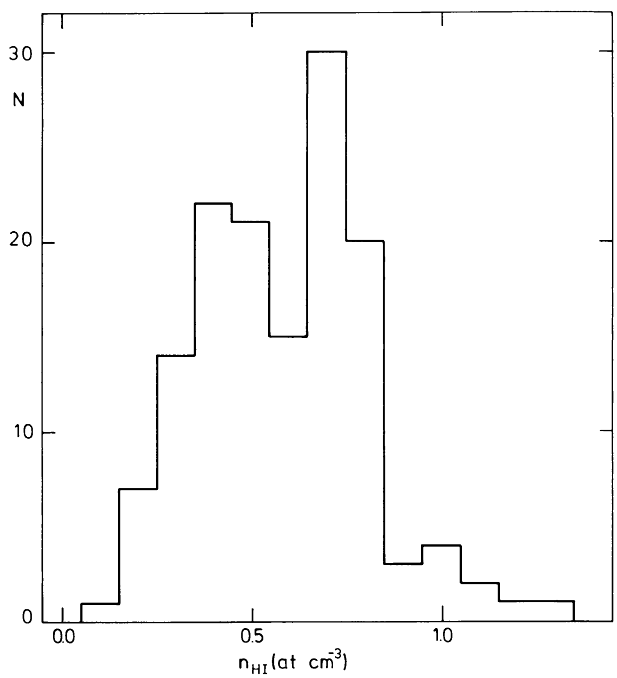

Fig. 7. Distribution of the average volume density, n_{HI}, of the H I surrounding the hole

uniform in terms of general noise level, the sensitivity of the survey drops sharply on the extreme northern and southern ends of the major axis. Thus, because of the limited extent of the survey, we miss H I holes at large radial distances around $\theta = 0°$ and 180°.

If we compare the distribution of holes in each of the four quadrants of M 31 we find the greatest number in the north-eastern and north-western quadrants, 38 and 49 holes respectively. This asymmetry in the distribution of holes is also present in the distribution of H I (cf. Paper II) and in the distribution of H II regions (cf. Fig. 2 of Pellet et al., 1978) which strengthens the suggestion that H I holes and regions of active star formation are correlated. The radial distribution of holes is shown in Fig. 6. For comparison we have also plotted the H I column density, σ_{HI}, as a function of radius, derived by averaging the total surface brightness maps in rings in the plane of the galaxy. Because averaging in this manner does not take warping of the plane into account (cf. Paper II) one should be cautious in interpreting this curve, especially at distances larger than about 16 kpc. The radial distribution of the holes follows more or less the H I distribution. Both curves peak around 10 kpc. A small secondary peak around 15 kpc can be seen which is related to the strong H I arm segment in the North. From a radius of about 15 kpc onwards the frequency of holes is a lower limit as a consequence of the limited coverage of the WSRT survey.

Figure 7 shows the distribution of ambient volume density, n_{HI}, for the H I surrounding the holes. The mean value for n_{HI} is 0.58 at cm^{-3} (cf. Paper II where $n_{HI} = 0.6$ at cm^{-3} was found, assuming the same inclination angle and scale height for the gas). The distribution of effective diameters of the holes is given in Fig. 8. The steep drop below 100 pc is caused by the limited linear resolution. If we approximate this size distribution by an exponential function we can extrapolate to small diameter objects. We estimate in this way that about 70 unresolved holes are missed by our survey. Figure 9 shows the distribution of axial ratios. Despite the fact that we have corrected for beam smoothing, we find that the peak lies at about 0.6, which is close to the axial ratio of the Westerbork beam at the declination of M31. Holes which are unresolved in one direction fall in the bin labelled 0.0. Otherwise, few holes show axial ratios less than 0.4, indicating that holes have at most moderate eccentricities. This is surprising, especially when considering the larger holes. If we take a value of 120 pc for the scale height of the H I gas around 10 kpc, the full width between points where the density has dropped to 10% is about 500 pc. So holes larger than 500 pc in diameter would correspond to cylinders in the flat disk of M 31 which are depleted of H I. The cylinders would show up as holes whose major axis is aligned with the major axis of M 31 and whose apparent ellipticity equals that of the galaxy, i.e. 0.22. To check this we have selected those holes which are larger than 500 pc. These holes indeed tend to align with the major axis of M 31, the best example being hole 69. The axial ratio, however, is in each case larger than 0.6. This might indicate that the gas is swept up in a more or less spherical shell

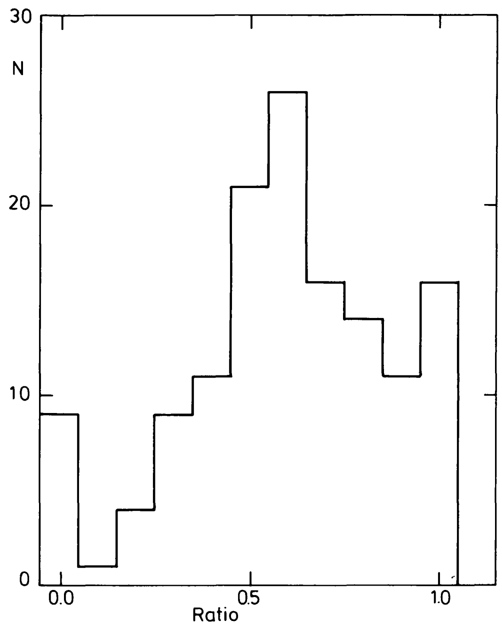

Fig. 9. Distribution of the axial ratios of the holes. Unresolved holes are placed in bin 0.0

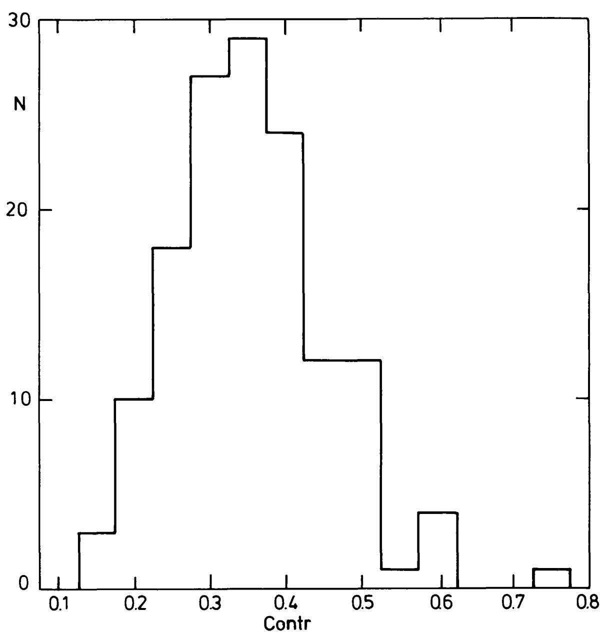

Fig. 10. Distribution of the parameter CONTR, which indicates the brightness temperature contrast of the hole to its surroundings in the channel map on which it is seen best

which expands into the halo, reaching high latitudes before breaking up.

Figure 10 shows the distribution of the parameter CONTR, the contrast of the hole to its surroundings on the channel map at velocity V_{HeI}. This distribution is peaked around a contrast of 0.35 and the full width at half maximum is about 0.2. Ideally a value of 0.5 is expected for each hole. The fact that the contrast of the holes peaks around a value of 0.35 instead of closer to a value of 0.5 does not mean that the hole is not devoid of neutral hydrogen. Because of the warping of the plane of M 31 (see Paper II) many lines-of-

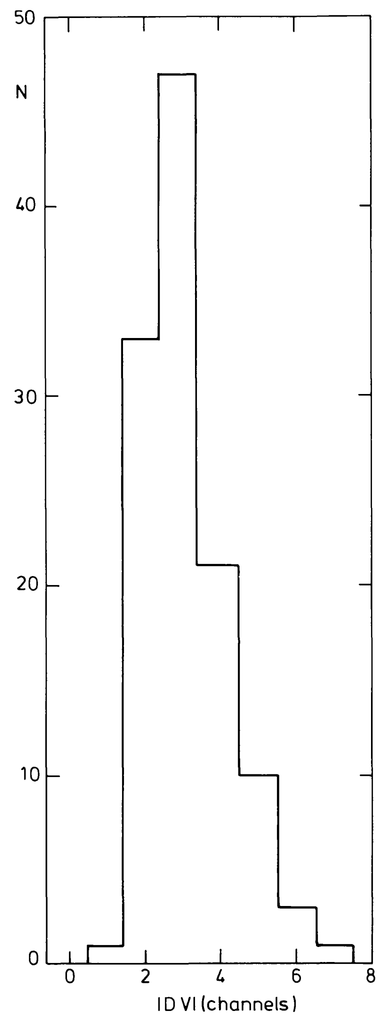

Fig. 11. Distribution of the absolute value of the expansion velocity expressed in number of channels. The channel separation is 4.1 km s^{-1}

sight sample both warp and disk H I, so the H I in the warp seen projected onto the disk reduces the contrast of a hole located in the disk. In a few cases the contrast is higher than 0.5. This can occur for those cases for which it is difficult to define the background intensity due to a steep gradient across the hole.

The expansion velocity measured for the holes of Type 2 and 3 is sharply peaked around 12 km s^{-1}. This is illustrated in Fig. 11. The coarse resolution of this histogram is due to the limited velocity sampling of the survey, 4.1 km s^{-1}. There are about equal numbers of holes of type $T=2$ showing red-shifted and blue-shifted expansion velocities, 41 and 34 respectively.

The histogram of the kinematic age of the holes shows that the ages fall between about 2.5 and 30 10^6 yr (Fig. 12), the mean age being about 10 10^6 yr. This range of ages is typical for OB-associations. It covers ZAMS lifetimes of stars which range from spectral type O5 to about B0. The indicative mass of H I which is absent from the volume of the hole ranges from $10^3\,M_\odot$ to $10^7\,M_\odot$. The peak value lies around $10^5\,M_\odot$ (see Fig. 13). Lastly the distribution of indicative energy is given in Fig. 14. This figure shows that the energy which is required to produce an H I hole ranges from about 10^{49} erg to 10^{53} erg. Thus the smaller holes could be produced by single supernova explosions, whereas the larger ones would require many supernovae each or some more

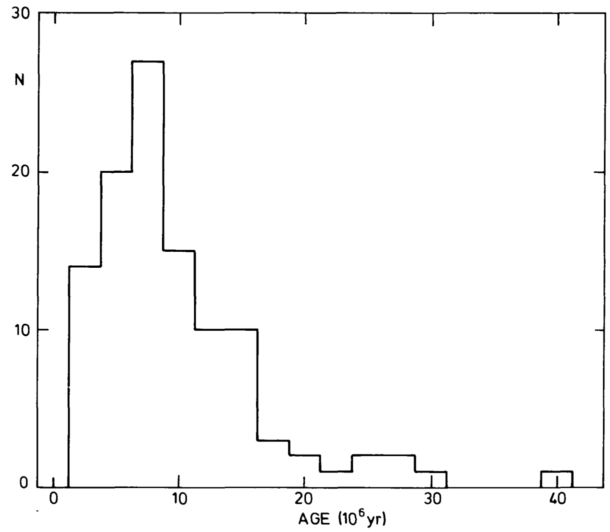

Fig. 12. Age distribution in units of 10^6 yr of the H I holes

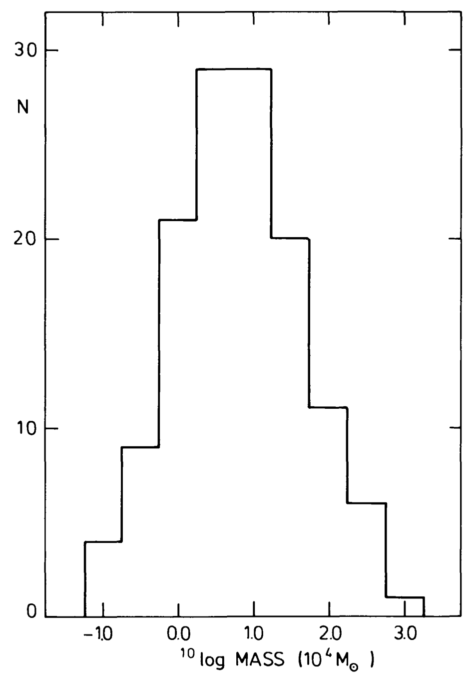

Fig. 13. Distribution of the H I mass which is absent, as defined in the text, in units of $10^4 M_{\odot}$

copious energy source. The distribution is peaked around energies of 10^{51} erg.

3.2. Relations between the properties of H I *holes and the quality, type, and class*

The quality, Q, assigned to a hole depends on how well the four selection criteria for H I holes are met. This rating is necessarily subjective and is difficult to quantify because the outcome depends on a multitude of factors, each influencing the result to a different degree. It is therefore worthwhile to check how strong the relations are between properties of holes such as the contrast, the diameter, etc. and Q. Only a few correlations are found and they are

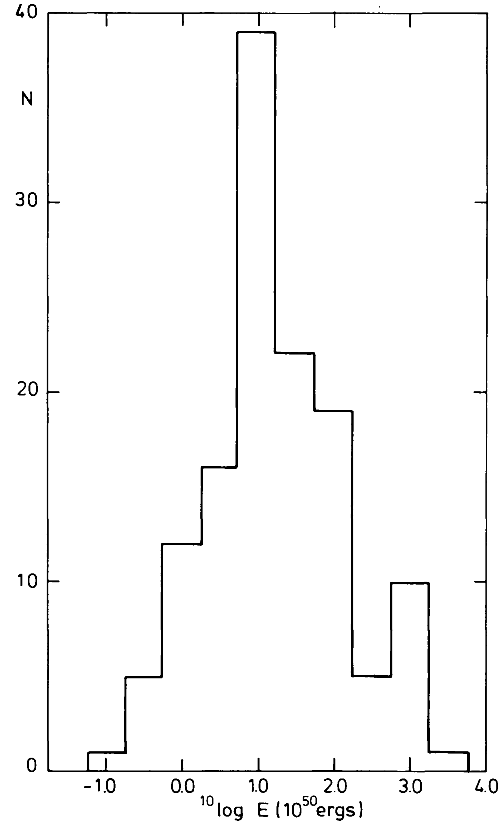

Fig. 14. Distribution of the energy required to produce the hole according to formula (2), in units of 10^{50} erg

presented in Fig. 15. This figure shows the mean values of the diameter, axial ratio, and contrast for each value of Q. The error bars in this figure represent r.m.s. deviations within each of the quality classes. The total number of $Q=1$ holes is 100 (71 %); there are 32 (23 %) $Q=2$ and 9 (6 %) $Q=3$ or very well defined holes. Despite the large spread of values for each property in each quality bin there is a clear tendency for the large diameter holes to be assigned higher qualities than the small ones. Also, low contrast holes are seldom assigned a high quality. The relation between Q and axial ratio, indicating that $Q=3$ holes are on the average rounder than $Q=1$ holes, results from the fact that, as we will show below, the effective diameter and the axial ratio are correlated.

The distribution of holes among the three different types is as follows: Type 1, 25 (18 %); Type 2, 75 (53 %); Type 3, 41 (29 %). The mean expansion velocity for Type 2 holes which show red-shifted H I is equal to those showing blue-shifted H I. Nor is there a difference in mean expansion velocity between Type 2 and Type 3 holes. There is a tendency for Type 1 holes to have a lower value for the mean n_{HI}, i.e. about 0.5 atoms cm^{-3} versus 0.6 atoms cm^{-3} for Type 2 and 3 holes. Additionally there is an indication that the contrast increases slightly in going from Type 1 to Type 3. Both findings can be understood as follows. For Type 1 holes H I is absent over the full velocity width of the neutral hydrogen, characterized by the velocity dispersion. This means that they are in general visible over a larger range in velocity than holes of Type 2 or 3 for which the H I is shifted in velocity only. This means that Type 1 holes can still be found in regions of relatively low surface density because they can be traced over this larger velocity range.

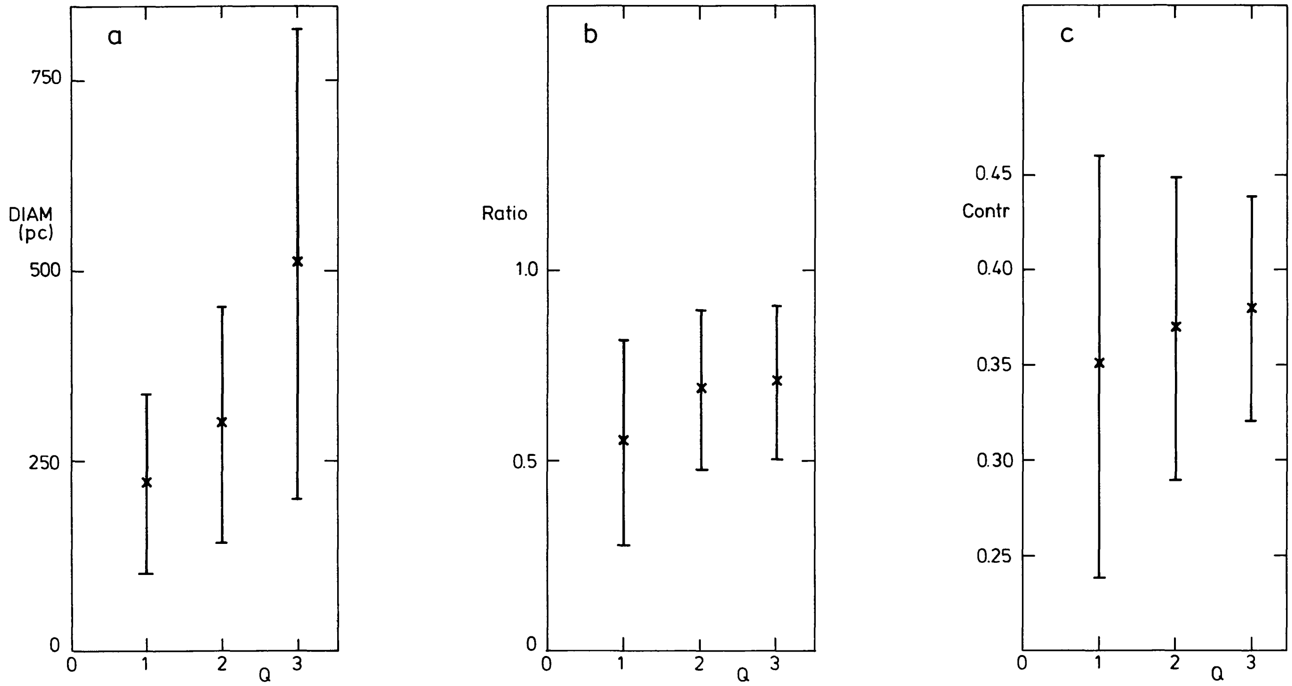

Fig. 15a. Effective diameter for each quality class, Q

Fig. 15b. Axial ratio for each quality class, Q

Fig. 15c. Contrast for each quality class, Q

Table 4a. Properties of H I holes as a function of the quality, Q

Quality	1	2	3
Total number	100	32	9
Fraction	71%	23%	6%
Mean diameter (pc)	220± 141	293± 154	510± 307
Mean contrast	0.35±0.11	0.37±0.08	0.38±0.06

Table 4c. Properties of H I holes as a function of the class, C

Class	*c*	*p*
Total number	103	38
Fraction	73%	27%
Mean diameter (pc)	220± 138	357± 227

Table 4b. Properties of H I holes as a function of the type, T

Type	1	2	3
Total number	25	75	41
Fraction	18%	53%	29%
Mean expansion velocity (km s^{-1})	–	13.2±4.8	13.9±3.7
Mean contrast	0.32±0.11	0.35±0.10	0.37±0.09
Mean n_{HI} (at cm^{-3})	0.51±0.29	0.61±0.21	0.58±0.19

The only relation which is evident for class C = "p" holes, i.e., holes which are only partially surrounded by H I, is that their effective diameter is on the average larger. This can be understood if one realizes that a small hole has a higher probability of being completely surrounded by H I in the channel maps than a larger hole. The relations found between the properties of H I holes and the quality, type, and class are summarized in Table 4.

3.3. *Correlations among the various other properties of the* H I *holes*

Since one might expect that there are certain relations between the various properties of the H I holes, for instance a dependence of some properties on galactocentric radius, we have searched the data in Tables 2 and 3 for such correlations. First we produced scatter diagrams to see if there was a relation between two properties. An example is given in Fig. 16, which shows a scatter diagram of the axial ratio of the holes versus their effective diameter. The broken line at 50 pc diameter indicates the resolution limit of our survey. As can be seen from the figure there are no large holes with high excentricity. If we assume that H I holes are the result of single or multiple supernova explosions then this figure tells us that as the holes expand they remain roughly spherical. The fact that the smaller holes tend to show a higher excentricity must be ascribed to a combination of two effects. Firstly for the smaller holes the result of the deconvolution for the beam is much more

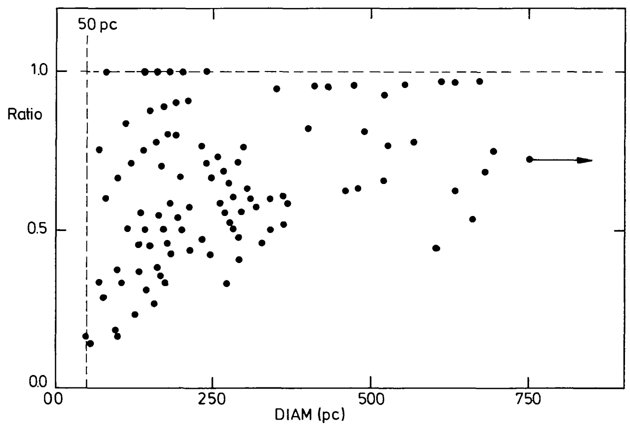

Fig. 16. Scatter diagram of the axial ratios versus diameters of the holes. The broken line at 50 pc indicates the resolution limit of the survey

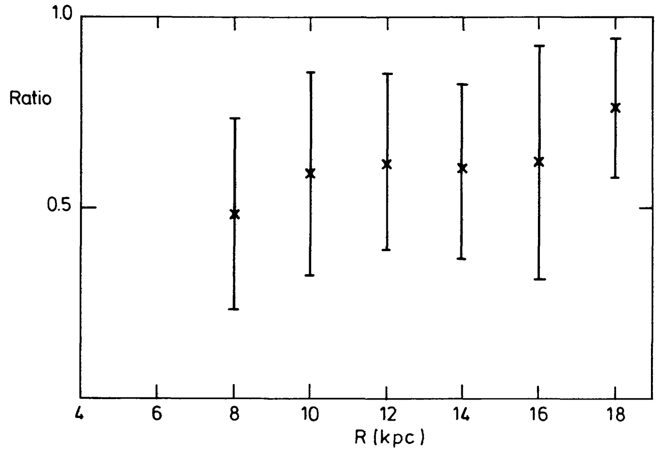

Fig. 18. As Fig. 17, for axial ratio versus R

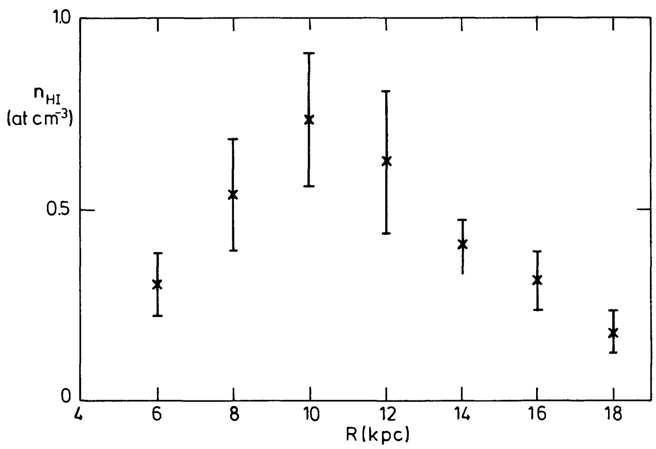

Fig. 17. Relation between average volume density and galactocentric distance. The holes were binned into 2 kpc wide rings in the plane of the galaxy. The error bars indicate the standard deviation from the mean for the holes which fall into each bin

critical. A small error in the measured dimensions of the hole will result in a large error in the deconvolved dimensions. That such an effect might be present is reflected in the distribution of the deconvolved axial ratios for the holes as shown in Fig. 9 and discussed above. Secondly the clumpiness of the gas introduces a scatter in the relative dimensions which is greater for small than for large holes.

We have produced diagrams like Fig. 16 for many of the derived and measured properties of the holes. However, in most diagrams the spread of the points is large making it difficult to distinguish trends. We have therefore grouped the holes into bins and plotted the mean values and standard deviations. We first checked on the existence of relations with R, the galactocentric distance. Figure 17 shows the relation between $n_{\mathrm{H\,I}}$ and R. We have binned the holes into 2 kpc rings. Within each bin the standard deviation is much larger than the measuring error. The relation between $n_{\mathrm{H\,I}}$ and R follows, as expected, the run of H I surface density as a function of R (cf. Fig. 6). There proved to be no relation between the diameter of the holes and galaxtocentric distance. In our Galaxy there is a tendency for H I shells to be larger at larger radii. This is discussed by Bruhweiler et al. (1980) and can be understood in terms of their model. One should be cautious in interpreting any dependence on radius in M 31 because most of our holes lie, due to the survey limits, in a narrow annulus of 10 kpc from the nucleus.

There is a tendency for holes to be rounder at large radii. This is shown in Fig. 18. Because there is no dependence of size on radius, the relation shown in Fig. 18 is not contaminated by the spurious correlation between axial ratio and diameter as discussed above. The result that holes are on average rounder at larger galactocentric radii can be understood if one realizes that the shear which is exerted on the hole by the differential rotation of the galaxy decreases with R.

Instead of searching for relationships between various properties and galactocentric distance R it might be physically more meaningful to see if the holes have different characteristics dependent upon their location with respect to the arms. The inclination of M 31 however, is such that individual arms can only be traced over relatively short distances, which makes it in many cases impossible to decide if a hole is located on the inside or the outside edge of an arm.

The last relation which we will discuss is the one between the diameter of the hole and the expansion velocity, DV. Figure 19 shows that there is a clear tendency for H I holes to be bigger if the expansion velocity is higher. In this figure the expansion velocity is binned into intervals of one half the velocity resolution (i.e. into bins which correspond to the channel separation of 4.1 km s^{-1}).

Checks on other combinations of properties of holes did not reveal any correlation which could not be traced back to two properties being so correlated as to suggested a causal relationship, or which could not be explained as being the result of selection effects.

4. Correlation of H I holes with H II regions and OB-associations

The H I holes are predominantly found in a broad annulus with a radius of about 10 kpc. The disk of M 31 shows in that area the highest activity in all regions of the electromagnetic spectrum. The 21-cm emission reaches its maximum intensity in this ring (see Paper I) and the star formation activity is highest there as is reflected by the distribution of H II regions as catalogued by Pellet et al. (1978) and by the location of OB-associations as described by van den Bergh (1964). As a consequence, the UV emission

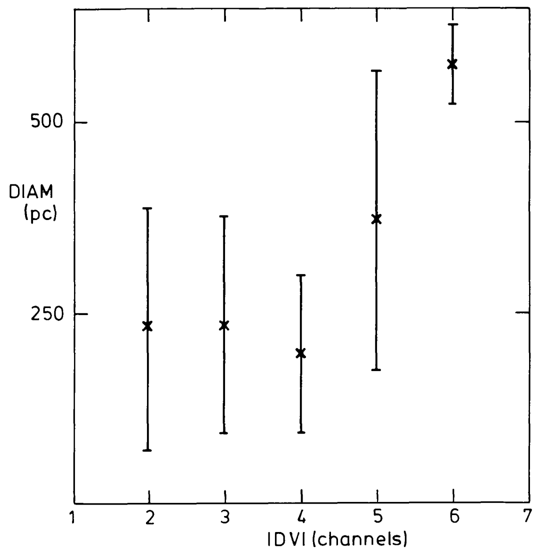

Fig. 19. Dependence of the diameter on the absolute value of the expansion velocity. One channel corresponds to 4.1 km s^{-1}

(Deharveng et al., 1980) is found to be restricted mainly to this annulus. The radio continuum emission also peaks there as is illustrated by the maps at 610 MHz published by Bystedt et al. (1984), at 1412 MHz by Walterbos et al. (1985), and at higher frequencies by the maps presented by Beck et al. (1980), and by Berkhuijsen et al. (1983). Further the infrared emission (Habing et al., 1984) is strongest in this ring and observations of CO emission have shown that in M 31 the molecules are also found in this annulus (Stark, 1979; Boulanger et al., 1981; Linke, 1981).

Because all these building blocks of the interstellar medium, holes, star formation regions, radio continuum, etc., are found in a rather narrow ring around 10 kpc the a priori probability that various features will overlap is high. This makes a test for a global correlation between H I holes and other constituents of the interstellar medium complex. Also such a procedure would make very limited use of the high resolution information which is obtained for the holes. If we adopt the picture of H I holes as being the result of a large scale process of star formation – perhaps a better description is the long term effect of an evolving group of massive stars culminating in their collective death as supernovae – then we should expect correlations with H II regions and OB-associations. This is supported by the fact that Heiles (1979) found a weak correlation of the H I shells and supershells with OB-associations in the Galaxy. It is further corroborated by the detailed correlations reported by Cowie et al. (1979, 1981).

For the H I holes found in M 31 we have checked the following correlations. We started with a detailed comparison with the OB-associations as listed by van den Bergh (1964) and with the H II regions as catalogued by Pellet et al. (1978). These comparisons were, as we will see below, the most meaningful. We tested for a correlation with dust (Hodge, 1980) but these results were ambiguous, mostly because the search for dust clouds is severely influenced by selection effects. Also, there appeared to be no relation between H I holes and open clusters (Hodge, 1979). Because some of the supershells in our Galaxy seem to correlate with radio loops (Hu, 1981; Heiles, 1984) we also checked the correlation of H I holes in M 31 with radio continuum emission. This radio continuum emission is intrinsically weak and the maps at 1412 MHz (Walterbos et al., 1985) and at 610 MHz (Bystedt et al., 1984) are patchy and have a relatively poor signal-to-noise ratio. One of the results from these radio continuum surveys is that the emission peaks are closely correlated with the H II regions listed by Pellet et al. (1978). Because of this correlation it is superfluous to correlate both the radio continuum emission and the H II regions with the H I holes. Since the H II region data is more complete we restricted ourselves to that correlation. We did not check the relation between holes and CO emission because at present no complete CO-survey exists for M 31 and because the areas which have been mapped (Boulanger et al., 1981; Linke, 1981) are observed at a relatively moderate angular resolution of about 1ʹ.7, which is equivalent to about 340 pc.

Recently a number of surveys have been performed to look for supernova remnants (SNRs). A total of 19 optically selected candidates have been found by D'Odorico et al., (1980) of which 11 sources are spectroscopically confirmed by Blair et al. (1981, 1982). We have checked the positions of these SNRs and of other objects which are suspected to be SNRs (Burger and Walterbos, private communication) but we found no coincidences of SNRs with H I holes. This might be understood as follows. The SNRs which were found in the surveys are still young compared to the H I holes. If we assume that holes are created by multiple supernova explosions then we do not expect to find supernovae in the holes when they reach the age at which we see them. Instead, the SNRs might mark the locations of future holes.

In comparing the holes with H II regions and OB-associations we proceeded as follows. For each hole we produced a channel map at a linear scale of 0.05 degree cm^{-1} and overlayed this map on the contour map of H II regions presented by Pellet et al. (1978, their Fig. 2) and on the maps of OB-associations published by van den Bergh (1964; see also the Atlas of the Andromeda Galaxy, Hodge, 1981), both maps brought to that same scale. For each hole we registered the H II regions and OB-associations which are spatially related. We used in this comparison the original channel maps which means that we took account of the detailed shape of each hole, instead of using the ellipses shown in Fig. 5. We quantified the measure of correlation by assigning overlap codes to the H II regions and OB-associations which coincide with the H I holes. If the hole is smaller than the H II region or OB-association then the codes are defined as follows. Code 1 indicates that the hole is spatially coincident with the H II region or OB-association. Code 2 indicates that the hole overlaps for more than about 50 % of its area with the H II region or OB-association. Code 3 means that there is an overlap of less than about 50 %. If the hole is larger than the H II region, or OB-association, the overlap of the latter with respect to the hole is measured. For a number of H II regions Deharveng and Pellet (1975a, b) have measured the radial velocity based on Hα interferogrammes. We list for each of these H II regions the velocity as given by Deharveng and Pellet (1975a).

The results of the correlation between H I holes on the one hand and H II regions and OB-associations on the other are summarized in Table 5.

Column 1: Number of the H I hole.

Column 2: Number of the H II region as listed by Pellet et al. (1978).

Column 3: Overlap code, as described in the text.

Table 5. Correlation of H I holes with H II regions and OB-associations

Name	Pellet			Deh-Pel		OB		H II
	No.	Code	EM	No.	V_{Hel} (km s^{-1})	No.	Code	Code
1	90	3	1			81	3	4
2						79	3	
3								
4	116	2	2			82	2	1
5	121	1	2			81	2	1
	126	1	1			81	2	3
	131	2	1			80	3	2
	130	2	2			80	3	2
6	121	2	2			81	3	1
	126	1	1			81	3	3
	131	1	1			80	1	2
	130	1	2			80	1	2
	134	1	3			80	1	2
	137	1	2			80	1	2
	138	1	1			80	1	2
	139	1	1			80	1	2
	140	3	1			80	1	3
	119	1	2			80	1	2
	115	2	3			80	1	2
	129	3	2			81	3	4
7						124	3	
						178	3	
8	152	3	1			82	1	1
	147	3	1			82	1	3
	129	3	2			82	1	4
	127	3	1			82	1	1
9						143	3	
10						143	3	
11						124	3	
12	173	3	2			78	1	1
	184	2	3			78	1	1
13	181	3	3			82	3	4
14						144	3	
15								
16	184	2	3			78	1	1
	182	2	2	69406	−574.4	78	1	1
	174	3	2			78	1	1
	183	2	1			78	1	1
	196	3	2			72	3	2
	189	3	2			72	3	2
17	190	2	2	69405	−438.4	122	1	2
	188	3	2	69404	−438.9	122	1	2
18	187	2	2					
19						83	3	
20	205	3	2			83	2	4
	204	3	1			83	2	4
21						145	3	
22								
23						122	3	

Table 5 (continued)

Name	Pellet			Deh-Pel		OB		H II
	No.	Code	EM	No.	V_{Hel} (km s^{-1})	No.	Code	Code
24	217	1	1			77	2	2
	220	2	2			77	2	4
	202	3	2			77	2	4
	214	3	1			71	3	3
25	212	2	3			84	1	2
26	220	2	2			77	3	4
27								
28	238	1	1			76	2	2
29	249	1	1			84	2	3
30								
31								
32								
33								
34								
35						86	1	
36						86	2	
37	310	3	1	50202	−410.7	68	2	2
	323	3	2			67	3	2
38								
39	323	2	2			67	2	2
	318	3	1			67	2	2
	316	3	1			67	2	2
40								
41	323	2	2			67	3	2
	318	3	1			67	3	2
42	354	1	2			66	1	1
	352	1	1			66	1	1
	348	3	1	50203	−407.4	66	1	1
43						26	3	
44								
45	371	1	1			26	2	3
	361	2	1			26	2	1
	375	1	1			27	3	1
	378	2	2			27	3	2
						89	3	
46	382	1	3			89	3	3
47								
48	386	2	1			27	3	1
	388	1	1			27	3	1
49	396	1	3			65	2	2
50	396	1	3			65	2	2
51						117	3	
52	407	2	1			117	3	4
53	412	3	1			28	3	1
	413	1	2			28	3	3
54	418	1	2			29	2	2
	420	2	1			29	2	1
	425	2	1			29	2	1
	422	3	2			29	2	1
	412	3	1			28	3	1

Table 5 (continued)

Name	Pellet			Deh-Pel		OB		H II
	No.	Code	EM	No.	V_{Hel} (km s^{-1})	No.	Code	Code
55	431	2	1			64	1	1
	433	3	1			64	1	1
	427	2	2			64	1	2
56	425	3	1			29	3	1
	422	3	2			29	3	1
	451	3	3			29	3	3
57	424	1	3			29	3	3
	428	3	3			29	3	4
	422	3	2			29	3	1
	451	3	3			29	3	3
						90	3	
58						174	3	
59	440	2	3					
	430	3	2					
	434	3	1					
60								
61	456	3	3			34	3	4
62	456	3	3			30	3	4
	451	3	3			30	3	1
	475	3	3			31	3	1
						34	1	
63	451	3	3			31	2	3
	475	3	3			31	2	1
	468	3	1			31	2	1
64	475	3	3			31	2	1
65						36	3	
66	504	3	3			32	3	1
	525	1	2			32	3	2
	530	3	1			32	3	1
	524	1	1	58303	−248.2	36	2	2
	523	1	3	58302	−247.8	36	2	1
	526	3	1	34	−269.4	36	2	1
	533	1	2			36	2	3
	534	2	2	67408	−253.1	36	2	2
	535	3	1	58301	−258.0	36	2	2
	542	3	1	58304	−247.6	37	3	1
	540	3	2	61805	−241.3	37	3	1
	532	2	1	61804	−243.4	36	2	1
67								
68								
69						116	3	
						172	3	
						171	3	
70						38	3	
71	578	3	3	58311	−225.2	38	2	1
	621	3	2			38	2	2
	540	3	2	33	−232.5	37	3	1
72	599	1	2	52605	−240.7	59	2	1
	577	2	1			59	2	1
	576	1	1			59	2	1
	589	3	1			59	2	1
	587	2	1			59	2	1
	592	3	1			59	2	1
	581	3	1			59	2	1

Table 5 (continued)

Name	Pellet			Deh-Pel		OB		H II
	No.	Code	EM	No.	V_{Hel} (km s^{-1})	No.	Code	Code
73	600	1	3			116	3	3
74	599	1	2	52605	−240.7	59	1	1
	597	2	1			59	1	1
	601	3	1			59	1	1
	603	1	1			59	1	1
	609	3	1			59	1	1
75	599	3	2	52605	−240.7	59	2	1
76	621	2	2			39	3	1
	606	3	1	27	−194.9	39	3	1
	607	3	1			39	3	1
	615	3	1	26	−195.4	39	3	1
	616	2	1			39	3	1
	617	3	1			39	3	2
						40	3	
77	621	3	2			40	3	1
	622	1	2			40	3	4
	624	2	1			40	3	3
	627	3	1			40	3	3
78	626	2	2			116	2	1
79	621	1	2			40	1	1
	624	3	1			40	1	3
	625	2	1			40	1	2
	629	3	1	61802	−206.5	40	1	1
80	631	1	3					
	641	2	2					
	644	3	1					
81								
82	646	2	2			115	3	2
83								
84	659	3	2			170	2	1
	660	3	1			170	2	1
85	677	3	2			58	3	1
86	677	1	2			58	1	1
87	621	2	2	58210	−175.5	41	3	2
	663	3	1			41	3	1
	667	2	1	17	−160.5	41	3	1
	675	1	1	18	−178.5	42	3	3
	682	3	1	58207	−167.7	42	3	1
88	677	2	2			58	2	1
	674	3	1			58	2	3
89	677	3	2			58	2	1
90	686	3	3			4	2	2
91	621	2	2	58209	−168.6	42	1	2
	682	1	1	58208	−168.8	42	1	1
	683	3	1	13	−164.3	42	1	1
	687	2	3	10	−167.7	42	1	1
						44	3	
92						58	3	
93	673	3	3			42	3	3
	692	3	2			42	3	4
94	687	3	3			44	1	3
	681	3	1	58205	−184.2	44	1	3

Table 5 (continued)

Name	Pellet			Deh-Pel		OB		H II
	No.	Code	EM	No.	V_{HeI} (km s^{-1})	No.	Code	Code
95								
96	687	2	3	10	−167.7	42	2	1
	690	2	1	58206	−181.5	42	2	1
97								
98						169	3	
99								
100	698	2	3			48	3	2
	705	3	3			48	3	2
	701	2	2			48	3	3
101								
102	706	3	2			57	2	4
103	704	1	2					
				68309	−176.0	3		
				68308	−188.8			
104						169	1	
105								
106						169	1	
107	705	1	3			48	2	2
	701	2	2			48	2	2
	722	3	2			48	2	1
	710	3	1			48	2	1
108						56	3	
109								
110	722	2	2			48	1	1
	716	3	1	6	−124.9	48	1	1
111								
112	718	2	1					
113	720	2	3			48	1	1
114						169	2	
115	720	2	3			48	2	1
	722	3	2			48	2	1
116						48	1	
117						48	2	
118				68314	−137.8			
119	754	3	2	68313	−127.7	55	2	3
120						167	3	
121	760	1	1					
	762	3	2					
122								
123	764	3	2					
	784	3	3					
124						167	3	
125								
126	775	3	2			54	2	1
	782	3	1			54	2	1
127	772	3	3			95	1	3
	794	3	3			95	1	1
	779	3	2			95	1	2
	787	2	2			95	1	1
	791	3	2			95	1	1
	796	3	2			95	1	1

Table 5 (continued)

Name	Pellet			Deh-Pel		OB		H II
	No.	Code	EM	No.	V_{Hel} (km s^{-1})	No.	Code	Code
128						54	2	1
129	806	1	3			49	1	1
	808	2	2			49	1	1
	804	2	1	61404	− 78.6	49	1	1
130	805	1	2			54	3	4
	821	1	2			54	3	4
	824	1	1			54	3	4
	825	1	1			54	3	4
	832	1	1			53	3	4
	835	2	1			53	3	3
	839	2	1	61401	− 94.7	53	3	1
	844	3	1			53	3	1
	842	2	1			53	3	2
	840	3	2			53	3	2
	834	2	3			53	3	3
	838	2	3			53	3	3
	850	3	2			53	3	2
	848	3	1			53	3	1
131								
132	811	3	1			45	2	4
	833	3	1	61403	−109.9	45	2	2
	830	1	2			46	1	3
133								
134						46	3	
135								
136								
137	857	3	3					
138	859	3	1			50	3	1
	856	3	2			50	3	2
139								
140								
141						52	3	

Column 4: Emission measure class, EM, of the H II region as specified by Pellet et al. (1978). S is the limiting surface brightness in 10^{-5} erg cm^{-2} s^{-1} sr^{-1}.

EM = 1: $S > 3.0$, EM = 2: $1.0 < S < 3.0$, EM = 3: $0.35 < S < 1.0$.

Column 5: Number of the H II region as given by Deharveng and Pellet (1975a).

Column 6: Radial velocity of the H II region in km s^{-1}.

Column 7: Number of the OB-association from the list of van den Bergh (1964).

Column 8: Overlap code as described above.

Column 9: Overlap code which indicates the relation between the H II region and the OB-association. Code 4 means that there is no overlap.

Van den Bergh (1964) groups the OB-associations into three age categories, based on their optical appearance. If one assumes that H I holes and OB-associations are causally related then one would expect that their age estimates agree. We checked whether there was a correlation by examining the associations for which both age estimates were present. There appeared to be no good correlation, although the same range of ages, i.e. from about 2.5 to 30 10^6 yr, is covered. This lack of correlation might be influenced both by the rather subjective method which was employed by van den Bergh to classify the associations, and by the manner in which we defined our age.

The radial velocities which were measured for a number of H II regions by Deharveng and Pellet (1975a) agree very well with the H I velocities. We have plotted in Fig. 20 the Hα velocities for the H II regions of all overlap codes against the central radial velocity of the hole, V_{Hel}. This figure shows that the velocity scales are in good agreement. The scatter around the expected relation indicated by the straight line is small and might be attributed to the

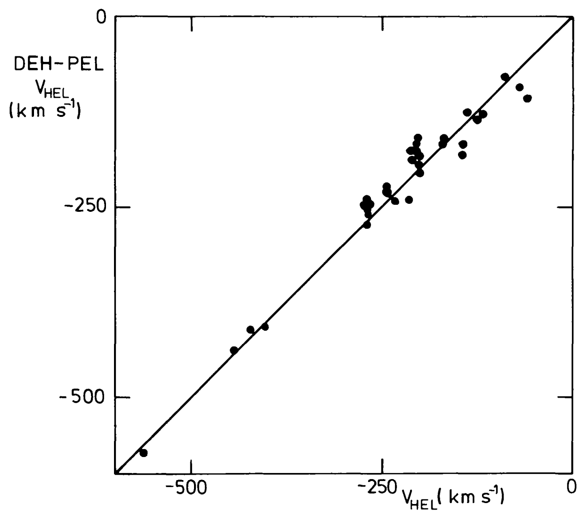

Fig. 20. Radial velocity of the H II regions which overlap with H I holes as measured by Deharveng and Pellet (1975a) on the basis of H α interferogrammes versus the velocity of the holes, V_{Hel}

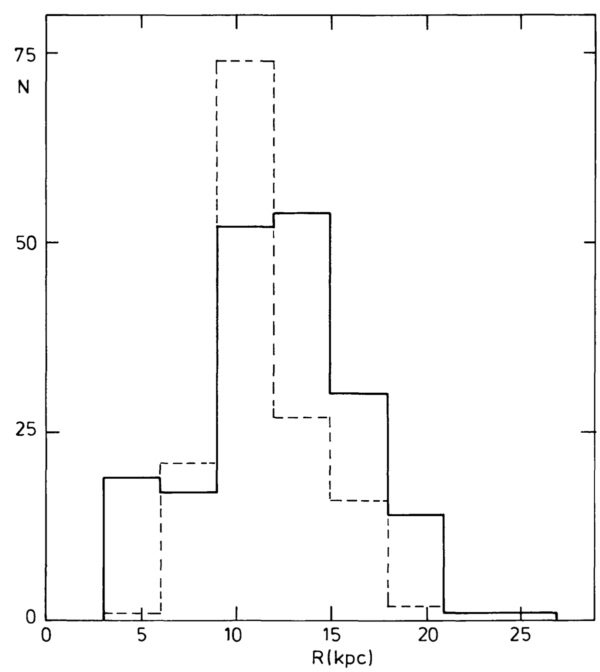

Fig. 21. Radial distribution of H I holes (dashed line), compared to the radial distribution of OB-associations (solid line) as given by van den Bergh (1964)

H II regions which follow the presumably expanding gas surrounding the hole. A more detailed comparison for the holes 66 and 87 is given by Brinks and Bajaja (1983b).

Although a correlation of H I holes with H II regions and OB-associations seems obvious it is nevertheless far from simple to quantify this correlation. This is mainly due to the fact that H I holes and other constituents of the interstellar medium are all found in the annulus with about 10 kpc radius. On a global scale we find that the enhanced star formation in the northern part of this annulus as indicated by a higher density of H II regions and OB-associations, seems to be reflected in a higher density of H I holes. The total number of OB-associations found by van den Bergh (1964) is 188 which is close to the total number of 141 H I holes. This latter value is a lower limit because of the survey limits of the H I observations. The surface density of holes and OB-associations thus appears to be the same, 0.2 objects kpc^{-2}, in the zone between radii of 7 and 16 kpc. The radial distribution and the size distribution for the OB-associations are compared with analogous data for the H I holes in Figs. 21 and 22. The radial distribution (Fig. 21) shows that the peak for OB-associations falls at a somewhat larger mean galactocentric distance. This might be caused by a selection effect. At a radius of 10 kpc the H I column density and thus the dust column density are highest. Internal absorption in this ring could lower the number of OB-associations found in this area. The relative lack of H I holes at larger distances is again due to the fact that the H I survey is incomplete. The size distributions of H I holes and the OB-associations (Fig. 22) are similar, both distributions having a maximum value for sizes of about 200 pc. The relative excess of OB-associations with diameters larger than about 300 pc might be a consequence of the fact that OB-associations which show subclustering were nevertheless listed as one entry in the OB catalogue.

The detailed spatial correlation of holes with H II regions and OB-associations which has resulted in Table 5 shows that there are many examples of good spatial coincidences. This is illustrated by the holes 79, 91, 129, and 132. In studying this correlation one gets the impression that there is a progression such that the smaller holes coincide with H II regions and the medium size holes with OB-associations. The large holes do not coincide with anything but show evidence for star formation along their border, which might indicate second generation star formation. However, it is easy to find in Table 5 counter examples of well defined holes which show no correlation at all with other objects.

It is difficult to quantify the correlation between H I holes on the one hand and H II regions and OB-associations on the other. This is for a large part due to the a priori probability for overlap of these objects. This probability depends on the diameter of the holes and increases with increasing diameter. We can estimate the relative overlap probability for the holes which we have found in our survey if we assume that this probability depends upon the area covered by each hole only. To improve the statistics we grouped the holes into diameter bins 100 pc wide. We then define

$$P_i = N_i D_i^2 \Big/ \sum_i N_i D_i^2 , \qquad (3)$$

where N_i is the number of holes in bin i and D_i the average diameter in this bin. P_i is then equal to the fraction covered by the holes in bin i of the total area covered by all holes found in the survey. Figures 23 and 24 show the histogram of the numbers of H II regions and OB-associations overlapping with holes, as a function of diameter. The dashed line indicates the distribution, normalized to the same total, which one would expect on the basis of the size distribution of the holes as observed (cf. Fig. 8) and the probability for overlap as calculated above. Both figures show that it is safe to conclude that at least for the smaller holes, i.e. smaller than about 250 pc, there is more overlapping than would be expected if there were no correlation at all. It should be noted that we included in this test H II regions and OB-associations of all overlap codes. We did not try to correct for the fact that holes might sometimes overlap with each other or for the fact that one OB-association or H II region might be associated with more than one hole. It proved statistically unjustified to produce histograms like Figs. 23 and 24 for each overlap code individually. It is anticipated that a Monte Carlo type simulation of the correlation between holes and other

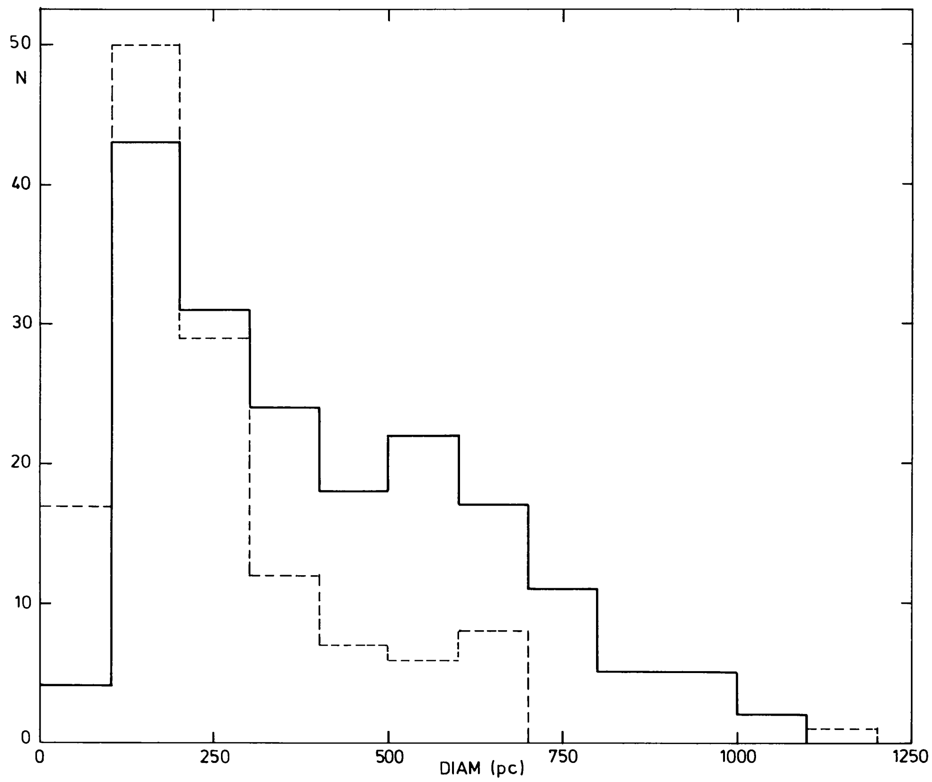

Fig. 22. Size distribution of H I holes (dashed line), compared to the size distribution of OB-associations (solid line) as given by van den Bergh (1964)

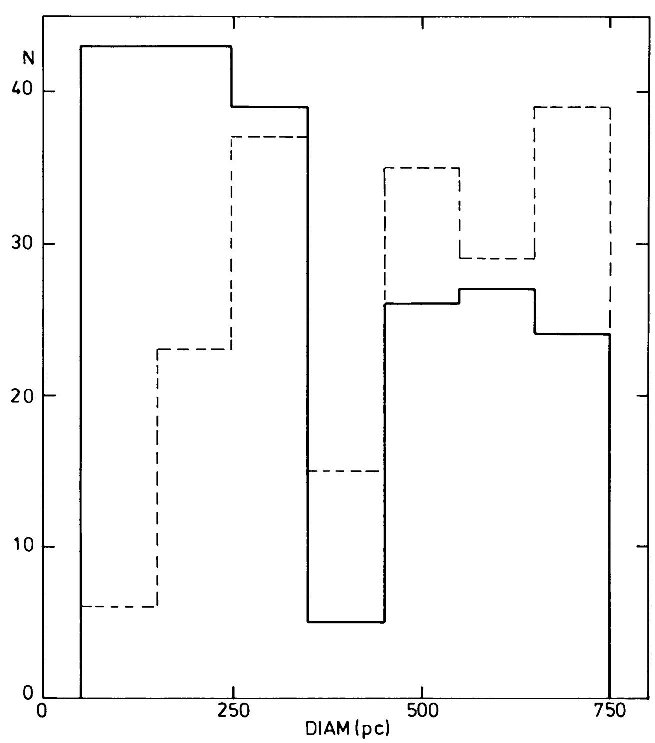

Fig. 23. Frequency distribution of the number of H II regions overlapping with H I holes as a function of the diameter of the holes. The dashed line indicates the normalized expected overlap frequency as explained in the text

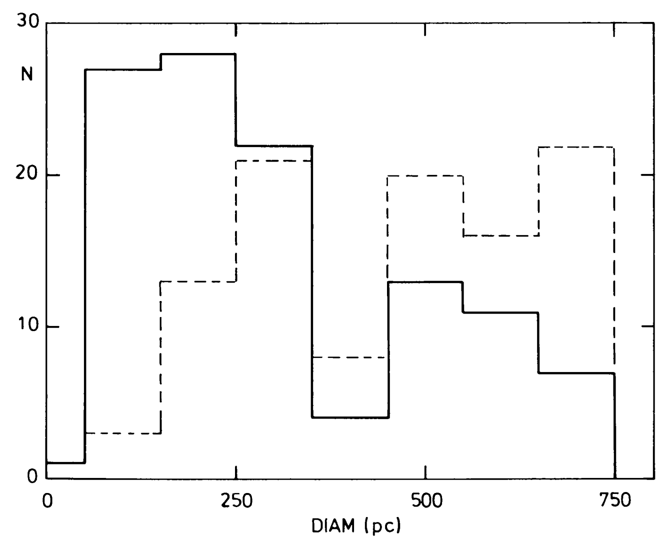

Fig. 24. As Fig. 23 for the overlap of OB-associations with H I holes

constituents of the interstellar medium might give more definite answers regarding these correlations, especially for the larger holes and perhaps also as function of overlap code.

5. Discussion

The ages of the holes as listed in Table 3 are kinematic ages, based on the effective diameters of the holes and their measured expansion velocities. As we have seen, these ages range between 2.5 and 30 10^6 yr. Van den Bergh (1964) finds for the OB-associations comparable ages. If we assume that the average age for the holes is about 10 to 20 10^6 yr then it follows that the hole formation rate is about 10^{-5} yr^{-1}. It is interesting to note that for a hole at a typical radius of about 10 kpc the time scale for distortion by shear is of the same order as the maximum age found for the holes, i.e. about 40 10^6 yr. However, the absence of holes with axial ratios smaller than 0.5 (cf. Fig. 9) suggests that shear can not be the main cause for the dissolution of holes.

Bruhweiler et al. (1980) adopt in their models for the shells found in the Galaxy a supernova rate of about 10^2 supernovae per shell. If we assume that the supernovae which create H I holes are all of Type II, then the Type II supernova rate for M 31 comes out to be about 1 per 1000 years, or about an order of magnitude less than the local value for the Galaxy and for M33 (Tammann, 1978; Berkhuijsen, 1983). This lower supernova rate in M 31 fits in with the lower overall activity of M 31 as compared to these other systems, reflected, for example, in the relatively low level of radio continuum (e.g. Berkhuijsen, 1977) and infrared emission (Habing et al., 1984; Walterbos and Schwering, 1986).

The volume filling factor which is derived for the holes which are found in the range from 7 to 16 kpc from the nucleus is about 1 %. This is much lower than a filling factor of 70–80 % as derived for the hot low density medium for the Galaxy by McKee and Ostriker (1977). If holes are the result of Type II supernova explosions then supernovae preferentially occur inside small volumes and not randomly distributed in M 31. This means that the fraction of hot gas which is produced by these supernovae is also restricted to the holes. As a consequence the hot medium, if due solely to this process, cannot form a structure of overlapping shells resulting in a tunneling network throughout large regions. Further in M 31 the supernova rate inferred on the basis of the holes is an order of magnitude less than the value adopted for the Galaxy by McKee and Ostriker (1977). This also suggests that the filling factor of the hot medium in M 31 is smaller than in our Galaxy and that the hot gas is thus confined to small volumes.

Larger holes and holes which are formed slightly out of the mean hydrogen layer can expand into the low density regions of the halo of M 31 and give rise to a galactic fountain (e.g. Bregman, 1980). This is reflected by the occurrence of Type 2 holes which show only one hemisphere, either blue-shifted or red-shifted. These holes might belong to the class of features in the Galaxy described as "Worms" (Heiles, 1984).

Many holes are located such that a line-of-sight to these objects traverses both warp and disk H I. About 30 holes are located in areas where the two systems, warp and disk, are well separated in velocity. These holes were used to check whether H I holes are present in the warp, and thus also whether star formation is presently going on in the warp. As we have seen in Paper II, the warp flares and the H I volume density in the warp decreases sharply as a function of distance from the nucleus, so we do not expect star formation to occur far into the warp. Combining the results from this paper and from Paper II, we conclude that indeed within our survey area no holes are located in the warp.

6. Conclusions

The results from this work can be summarized as follows:

1) In the area of M 31 surveyed by the WSRT 141 regions are located – H I holes – which are characterized by an absence of neutral hydrogen. The size of these holes ranges from about 100 pc to 1 kpc.

2) The holes are located mainly in an annulus with a radius of 10 kpc, i.e. restricted to the same general area as the H II regions, OB-associations, infrared and radio continuum emission, etc. There are no holes found in the warped parts of M 31.

3) The most frequently found expansion velocity for the holes is about 12 km s^{-1}. About 50 % of the holes show only one hemisphere, which is either red-shifted or blue-shifted.

4) The H I mass estimated to be removed from a hole ranges from about 10^3 to 10^7 $M_\odot$. The energy needed to produce the holes lies in the range from 10^{49} to 10^{53} ergs. The kinematic ages are about 2.5 to 30 10^6 yr. These ages are in agreement with age estimates for OB-associations.

5) Within the survey area there is no indication that the diameter of holes increases with galactocentric radius, in contrast to what is found for the shells in the Galaxy. We do find a tendency that holes at larger radii are rounder, possibly as a result of less shear.

6) For the holes which are smaller than about 300 pc we are confident that they are correlated with OB-associations and with H II regions. For larger holes, a correlation is suggested by the data but may be partly apparent as a result of the a priori probability for overlap which increases with increasing diameter of the holes. There appears to be no correlation with SNRs.

7) Our data indicate a production rate of 1 hole every 10^5 yr. Assuming an average number of 10^2 supernovae per hole (Bruhweiler et al., 1980), we find a supernova rate of 10^{-3} yr^{-1} or about 10^{-14} pc^{-3} yr^{-1}, which is an order of magnitude lower than the corresponding local value for the Galaxy and the value estimated for M33.

8) The filling factor of the holes is about 1 %. This is much less than the value for the hot low density medium which is expected by McKee and Ostriker (1977) for the Galaxy. Our results indicate that if the hot low density medium originates from Type II supernovae the hot gas in M 31 can not form a tunneling network, but is restricted mainly to the volumes characterized by the holes.

Acknowledgements. We would like to acknowledge the extensive help which we have received from Mrs. H. Versteege-Hensel who assisted us in various stages of this project. We thank Drs. W. Burton, A. Bosma, and H. van der Laan who have provided us with comments which have improved the presentation of this paper. We are especially grateful to Dr. C. Norman for many lively discussions on this subject and to Dr. W. Shane for his detailed comments on the manuscript. The drawings were produced by Mr. J. Ober and the photographs by Mr. W. Brokaar.

E. Brinks was supported financially by the Netherlands Foundation for Astronomical Research (ASTRON). The Westerbork Synthesis Radio Telescope is operated by the Netherlands Foundation for Radio Astronomy (SRZM). Both foundations are supported by the Netherlands Organization for the Advancement of Pure Research (ZWO). E. Bajaja gratefully acknowledges a Visitor's grant from ZWO and travel funds provided by CONICET.

References

Arp, H.: 1964, *Astrophys. J.* **139**, 1045

Baade, W., Swope, H.H.: 1963, *Astron. J.* **68**, 435

Baade, W., Arp, H.: 1964, *Astrophys. J.* **139**, 1027

Beck, R., Berkhuijsen, E.M., Wielebinski, R.: 1980, *Nature* **283**, 272

Berkhuijsen, E.M.: 1977, *Astron. Astrophys.* **57**, 9

Berkhuijsen, E.M.: 1983, *Astron. Astrophys.* **120**, 147

Berkhuijsen, E.M., Wielebinski, R., Beck, R.: 1983, *Astron. Astrophys.* **117**, 141

Blair, W.P., Kirshner, R.P., Chevalier, R.A.: 1981, *Astrophys. J.* **247**, 879

Blair, W.P., Kirshner, R.P., Chevalier, R.A.: 1982, *Astrophys. J.* **254,** 50

Boulanger, F., Stark, A.A., Combes, F.: 1981, *Astron. Astrophys.* **93**, L1

Braunsfurth, E., Feitzinger, J.V.: 1983, *Astron. Astrophys.* **127**, 113

Bregman, J.N.: 1980, *Astrophys. J.* **236,** 577

Brinks, E.: 1981, *Astron. Astrophys.* **95**, L1

Brinks, E., Bajaja, E.: 1983a, in *Internal Kinematics and Dynamics of Galaxies*, IAU Symp. **100**, ed. E. Athanassoula, Reidel, Dordrecht, p. 139

Brinks, E., Bajaja, E.: 1983b, in *Proc. Leiden Workshop Southern Galactic Surveys*, *Astrophys. Space Science Library* **105**, eds. W.B. Burton, F.P. Israel, Reidel, Dordrecht, p. 247

Brinks, E., Burton, W.B.: 1984, *Astron. Astrophys.* **141**, 195 (Paper II)

Brinks, E., Shane, W.W.: 1984, *Astron. Astrophys. Suppl.* **55**, 179 (Paper I)

Bruhweiler, F.C., Gull, T.R., Kafatos, M., Sofia, S.: 1980, *Astrophys. J. Letters* **238**, L27

Bystedt, J.E.V., Brinks, E., de Bruyn, A.G., Israel, F.P., Schwering, P.B.W., Shane, W.W., Walterbos, R.A.M.: 1984, *Astron. Astrophys. Suppl.* **56**, 245

Cash, W., Charles, P., Bowyer, S., Walter, F., Garmire, G., Riegler, G.: 1980, *Astrophys. J. Letters* **238**, L71

Castor, J., McCray, R., Weaver, R.: 1975, *Astrophys. J. Letters* **200**, L107

Chevalier, R.A.: 1977, *Ann. Rev. Astron. Astrophys.* **15**, 175

Cowie, L.L., Hu, E.M., Taylor, W., York, D.G.: 1981, *Astrophys. J. Letters* **250**, L25

Cowie, L.L., Songaila, A., York, D.G.: 1979, *Astrophys. J.* **230**, 469

Cox, D.P., Smith, B.W.: 1974, *Astrophys. J. Letters* **189**, L105

Deharveng, J.M., Jakobsen, P., Milliard, B., Laget, M.: 1980, *Astron. Astrophys.* **88**, 52

Deharveng, J.M., Pellet, A.: 1975a, *Astron. Astrophys. Suppl.* **19**, 351

Deharveng, J.M., Pellet, A.: 1975b, *Astron. Astrophys.* **38**, 15

de Vaucouleurs, G., de Vaucouleurs, A., Corwin, H.G., Jr.: 1976, *Second Reference Catalogue of Bright Galaxies*, University of Texas Press, Austin

D'Odorico, S., Dopita, M.A., Benvenuti, P.: 1980, *Astron. Astrophys. Suppl.* **40**, 67

Elmegreen, B.G., Chiang, W.-H.: 1982, *Astrophys. J.* **253**, 666

Georgelin, Y.M., Georgelin, Y.P., Laval, A., Monnet, G., Rosado, M.: 1983, *Astron. Astrophys. Suppl.* **54**, 459

Habing, H.J., Miley, G., Young, E., Baud, B., Boggess, N., Clegg, P.E., de Jong, T., Harris, S., Raimond, E., Rowan-Robinson, M., Soifer, B.T.: 1984, *Astrophys. J. Letters* **278**, L59

Heiles, C.: *Astrophys. J.* **229**, 533

Heiles, C.: 1984, *Astrophys. J. Suppl.* **55**, 585

Heiles, C., Habing, H.J.: 1974, *Astron. Astrophys. Suppl.* **14**, 1

Hodge, P.W.: 1979, *Astron. J.* **84**, 744

Hodge, P.W.: 1980, *Astron. J.* **85**, 376

Hodge, P.W.: 1981, *Atlas of the Andromeda Galaxy*, (Univ. of Washington Press, Seattle

Hu, E.M.: 1981, *Astrophys. J.* **248**, 119

Linke, R.A.: 1981, in *Extragalactic Molecules*, eds. L. Blitz, M.L. Kutner, NRAO, Green Bank, p. 87

McKee, C.F., Ostriker, J.P.: *Astrophys. J.* **218**, 148

Meaburn, J.: 1980, *Monthly Notices Roy. Astron. Soc.* **192**, 365

Pellet, A., Astier, N., Viale, A., Courtès, G., Maucherat, A., Monnet, G., Simien, F.: 1978, *Astron. Astrophys. Suppl.* **31**, 439

Shostak, G.S., van Woerden, H.: 1983, in *Internal Kinematics and Dynamics of Galaxies*, *IAU Symp.* **100**, ed. E. Athanassoula, Reidel, Dordrecht, p. 33

Simien, F., Athanassoula, E., Pellet, A., Monnet, G., Maucherat, A., Courtès, G.: 1978, *Astron. Astrophys.* **67**, 73

Stark, A.A.: 1979, Ph.D. thesis, Princeton

Tammann, G.A.: 1978, *Mem. Soc. Astron. Ital.* **49**, 315

Tenorio-Tagle, G.: 1981, *Astron. Astrophys.* **94**, 338

Tenorio-Tagle, G.: 1984, *Publ. Astron. Inst. Czech. Acad. Sci.* **56**, 168

Tenorio-Tagle, G., Beltrametti, M., Bodenheimer, P., Yorke, H.W.: 1982, *Astron. Astrophys.* **112**, 104

Tomisaka, K., Habe, A., Ikeuchi, S.: 1981, *Astrophys. Space Sci.* **78**, 273

van den Bergh, S.: 1964, *Astrophys. J. Suppl.* **9**, 65

Walterbos, R.A.M., Brinks, E., Shane, W.W.: 1985, *Astron. Astrophys. Suppl.* **61**, 451

Walterbos, R.A.M., Schwering, P.B.W.: 1986, in *Light on Dark Matter*, ed. F.P. Israel (in press)

Weaver, R., McCray, R., Castor, J., Shapiro, P., Moore, R.: 1977, *Astrophys. J.* **218**, 377

Wild, J.P.: 1970, *Australian J. Phys.* **23**, 113